

# A Sensorless Induction Machine Drive

- An implementation study

A Master's thesis by Håkan Carlsson and Johan Bergerlind



Department of Energy and Environment  
CHALMERS UNIVERSITY OF TECHNOLOGY  
Göteborg, Sweden 2006



**Aros electronics AB**

Möndal, Sweden 2006



## Abstract

This Master's thesis describes a DSP implementation of the Statically Compensated Voltage Model (SCVM) algorithm for sensorless induction machine control. The algorithm is aimed to be implemented in a 16-bit fixed-point processor.

In general, low speed operation with voltage model based control systems is problematic, especially when in generator mode. In generator mode with the load at nominal torque, the implemented design fails already at 7.5 Hz. With a lower load, 2 Nm or 54 % of nominal, the drive is able brake it to almost zero, but the speed accuracy is low. On the other hand, if the motor operates in motor mode, low speed is less problematic. Experiments show that this implementation can handle variations in stator resistance from -37 % up to +60 % with stable low speed operation and variations of at least  $\pm 60$  % at nominal speed. Stable operation for all speeds is possible even during an increase of rotor resistance by 60 %, but the speed accuracy will be reduced by approximately 2 %. The rotor resistance may decrease by 58 % at low speed and by 53 % at nominal speed before the drive destabilizes. The total leakage inductance can vary at least  $\pm 30$  % without noticeably affecting the system.

The thesis project is conducted in association with Aros electronics AB.



## **Acknowledgments**

We would like to thank our supervisor at Aros electronics AB, Ph.D. Mikael Alatalo, for his unwavering support, help and encouragement. We also extend our thanks to our examiner, associate professor Torbjörn Thiringer, and to Ph.D. Andreas Petersson for their help with theoretical questions and alternative approaches to problems. Professor Lennart Harnefors and Ph.D. Rolf Ottersten has through their work with the SCVM and to some extent also by helping us directly inspired and motivated our work. The work of Ph.D. student Oskar Wallmark has also been a source of inspiration during this thesis work.

Last but certainly not least, a warm thanks to all employees at Aros electronics AB for their kindness and support, making us feel most welcome during our thesis work.



# Contents

<b>1</b>	<b>Introduction</b>	<b>1</b>
1.1	Purpose . . . . .	1
1.2	Goal . . . . .	1
1.3	Sources . . . . .	2
1.4	Structure . . . . .	2
<b>2</b>	<b>Induction Motor Basics</b>	<b>3</b>
2.1	Mechanical Construction . . . . .	3
2.2	Mathematical Circuit Models . . . . .	3
2.3	Principle of Operation . . . . .	6
<b>3</b>	<b>Vector Control</b>	<b>8</b>
3.1	Space Vectors . . . . .	8
3.2	Synchronous Coordinates . . . . .	9
3.3	Motor Control . . . . .	9
3.4	Sensorless Motor Control . . . . .	9
<b>4</b>	<b>Sensorless Control Algorithm</b>	<b>12</b>
4.1	Improved Statically Compensated Voltage Model . . . . .	12
4.2	Parameter Sensitivity of the SCVM . . . . .	14
4.3	Known Limitations of the SCVM . . . . .	14
<b>5</b>	<b>Simulations</b>	<b>16</b>
5.1	Motor Model . . . . .	16
5.2	Model Verification . . . . .	18
5.3	Control System Model . . . . .	18
5.4	The Improved SCVM Model . . . . .	20
5.5	Simulation Results . . . . .	21
5.6	New Parameters . . . . .	23
5.7	Simulation Conclusions . . . . .	24
<b>6</b>	<b>Implementation</b>	<b>25</b>
6.1	Hardware . . . . .	25
6.1.1	Controller Card . . . . .	25

6.1.2	Motor . . . . .	26
6.2	Software . . . . .	26
6.3	Data Acquisition . . . . .	26
6.4	Implementation Issues . . . . .	27
<b>7</b>	<b>Results</b>	<b>28</b>
7.1	Speed Step Response . . . . .	28
7.2	Slow Speed . . . . .	28
7.2.1	Slow Speed Limit . . . . .	28
7.2.2	Reversing . . . . .	31
7.3	Parameter Sensitivity . . . . .	36
7.3.1	Deviations in Stator Resistance . . . . .	36
7.3.2	Deviations in Rotor Resistance . . . . .	42
7.3.3	Deviations in Leakage Inductance . . . . .	46
<b>8</b>	<b>Conclusions</b>	<b>50</b>
8.1	Goal Fulfilment . . . . .	50
8.1.1	Stable Operation up to Nominal Speed . . . . .	50
8.1.2	Stable Operation up to Twice the Nominal Torque . . . . .	50
8.1.3	Stable Operation during Acceleration and Decelera- tion with an Arbitrary Load . . . . .	50
8.1.4	Stable Operation during Parameter Variations . . . . .	50
8.2	Further Work . . . . .	51
<b>A</b>	<b>Measurement of Motor Parameters</b>	<b>52</b>
A.1	Locked Rotor Test . . . . .	53
A.2	No-load Test . . . . .	54

# Chapter 1

## Introduction

Vector control of induction machines (IM:s) is a well known tool for advanced control of AC-machines. This method of control requires knowledge of the rotor flux angle. Traditionally, this has been derived using current measurements and information about the rotor speed, measured by a device mounted on the shaft of the machine. However, there are several problems involved with the speed measurement. The measuring device, often an encoder or a resolver, is expensive and adds another component that may fail in the system. The drive will also be sensitive to disturbances and harsh operational environments. The measuring device also need space for mounting, which may prove problematic in some applications, as well as communication between the device and the control system. Careful mounting and alignment are often necessary, further increasing the production costs. The problems concerning rotor speed measurement have spurred a development of methods for sensorless flux angle estimation and thus advanced control of the machine without mechanical sensors.

### 1.1 Purpose

This Master's thesis describes the implementation of the Statically Compensated Voltage Model flux- and speed-sensorless control strategy for an induction machine. Some basic vector control theory is also covered.

### 1.2 Goal

The goal is to achieve a sensorless IM drive that enables stable operation

- up to the nominal speed.
- up to twice the nominal torque.
- during acceleration and deceleration with an arbitrary load.

- during variations in rotor and stator resistance up to 60 % and in the total leakage inductance up to 30 %.

### 1.3 Sources

There is much research done on the subject of sensorless control. Numerous articles and papers has been published. Earlier work at Aros electronics AB includes a Master's thesis by Anders Ottergren [1], "Evaluation of speed observers for an induction machine". This paper is considered in Chapter 4.

Professor Lennart Harnefors has written two very informative compendia about control of variable speed drives, [2] and [3]. The second is partly an extended version of the first, covering also control of power electronic converters. Harnefors presents a promising algorithm called the Statically Compensated Voltage Model or SCVM. This is the approach we will further study.

### 1.4 Structure

The theory of vector control is covered in Chapter 3 to give an introduction to the subject of field oriented motor drives. The SCVM method for sensorless control is discussed in Chapter 4. In Chapter 5 the control system and the mathematical model of the motor is described and implemented using Matlab Simulink. The results of the different simulations are displayed and discussed here as well. The main part of this thesis is the implementation, Chapter 6, and the results here of are described in Chapter 7. The report is ended with a conclusion part, Chapter 8.

## Chapter 2

# Induction Motor Basics

As a background to motor control, some basic induction motor principles are explained.

### 2.1 Mechanical Construction

The fundamental parts of the induction motor are the stator and the rotor. In the IM, unlike the DC-machine, the rotor conductors are short-circuited and are, compared to earlier constructions of plain copper wiring, nowadays mostly made of solid aluminum. In most cases the rotor slots are skewed which reduces nonlinear effects and in turn harmonic content of the flux, with less torque pulsations and lower acoustic noise as a result [2]. The rotor is indirectly propelled by the magnetic field produced by the stator, hence induction motor. This makes it important for the airgap between the stator and rotor to be small in order to limit the flux leakage. Larger airgap means higher losses in the stator windings, giving a lower efficiency.

### 2.2 Mathematical Circuit Models

A classical way to model the induction motor is the single phase "T model", see figure 2.1 [4]. It consists of the resistance and inductance of the stator and rotor. The magnetizing impedance is represented by an inductance. Sometimes the active power loss in the core is included in the model, but hardly ever in simulations. If included, it is represented by a resistance,  $R_c$ , connected in parallel or in series with the magnetizing inductance  $L_m$ . In this thesis it is excluded, with exception from the parameter calculations in appendix A.

Another suitable equivalent model is the "inverse- $\Gamma$  model", see figure 2.2. Contrary to the T model, all leakage inductance is transferred to one side, the stator side.

There is a direct translation between T and inverse- $\Gamma$  parameters:

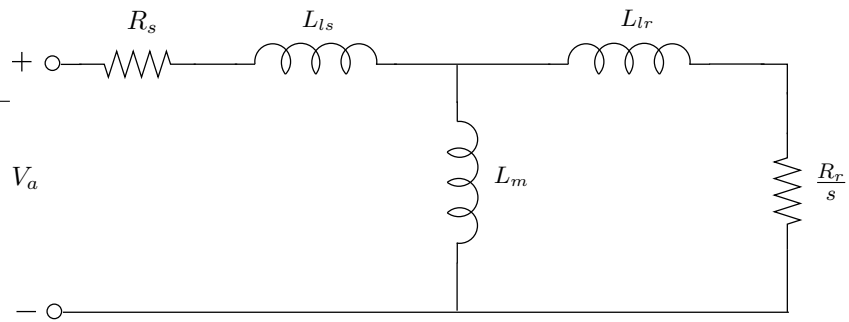


Figure 2.1: Single phase T model of an induction motor.

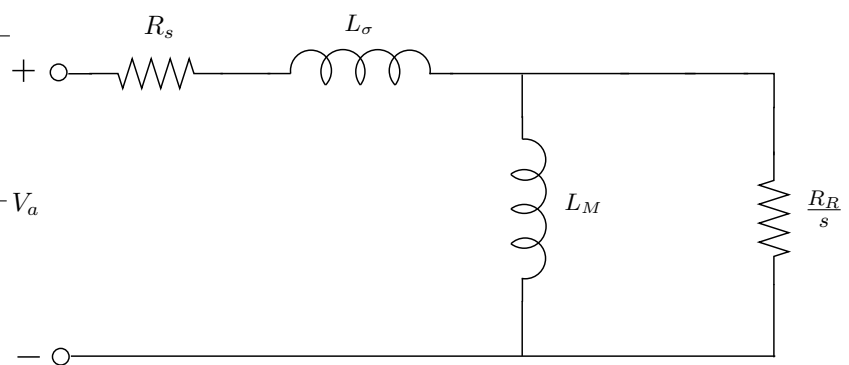


Figure 2.2: Single phase inverse- $\Gamma$  model of an induction motor.

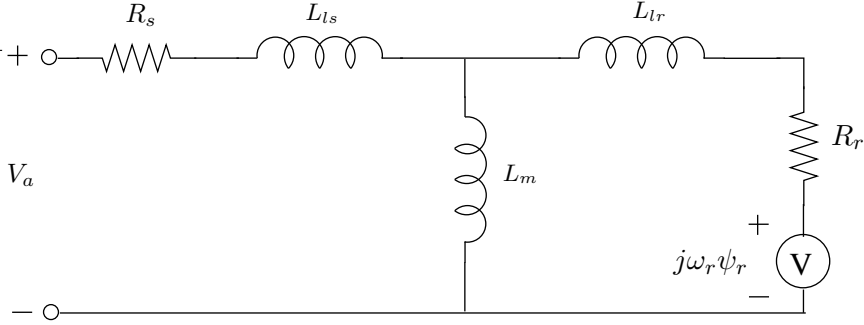


Figure 2.3: Single phase dynamic T model of an induction motor.

$$L_\sigma = L_s - \frac{L_m^2}{L_r} \quad (2.1)$$

$$L_M = \frac{L_m^2}{L_r} \quad (2.2)$$

$$R_R = R_r \left( \frac{L_m}{L_r} \right)^2 \quad (2.3)$$

$$\psi_R = \psi_r \frac{L_m}{L_r} \quad (2.4)$$

where  $L_s = L_{ls} + L_m$  and  $L_r = L_{lr} + L_m$ .

Since they are steady-state set-ups, these models are not feasible for analysis of the dynamic behavior of the IM. Instead, two models valid for transient analysis are used [3]. In figure 2.3 and 2.4, the effective rotor resistance dependent of the slip is replaced with a voltage source corresponding to the back EMF. For a more detailed description of back EMF, see Section 2.3.

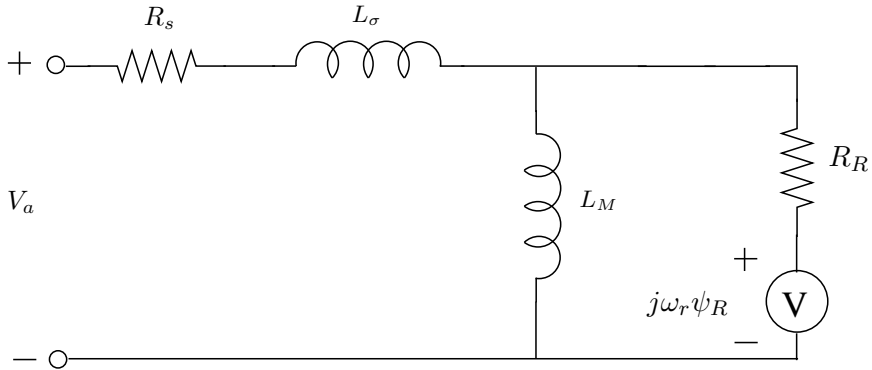


Figure 2.4: Single phase dynamic inverse- $\Gamma$  model of an induction motor.

## 2.3 Principle of Operation

The three-phase induction motor is based upon electro-magnetic interaction between the stator and rotor. As alternating voltages displaced 120 degrees to each other are applied to the stator windings, stator currents are formed. A rotating magnetic field with varying flux density is generated. The magnetic flux induce a voltage over the rotor resulting in a current through the rotor windings. As there is a magnetic field present, the flowing current will generate a force acting upon the rotor windings, thus producing an electro-dynamic torque.

The rotor voltage is induced as long as the stator field is not moving with the same speed as the rotor. As the rotor accelerates, the induced voltage and current will drop. As an effect the torque is reduced. If the machine is not loaded, the rotor practically keeps the same speed as the stator field. Thus the speed difference, called slip speed or lag, will be small and the torque almost zero. If the motor is loaded, the rotor speed will be lower and the torque increases until the load is matched according to equation (2.5). If the load is driving the rotor faster than the stator field, the voltage over the rotor change polarity and the produced torque will be in the reverse direction compared to the stator field movement. This will brake the load [5]. The mechanical speed of the motor is often represented by

$$\omega_r = \frac{(T_e - T_L)}{J} e^{-Bt/J} \quad (2.5)$$

where  $T_e$  is the electrodynamic torque,  $T_L$  the applied load,  $J$  the moment of inertia and  $B$  the viscous friction. figure 2.5 is a sketch of the AC induction motor torque and steady-state torque limits due to thermal limitations in the machine. The maximum speed noted in figure 2.5 is due to mechanical construction limitations of the rotor.

The rotor current is producing a magnetic field of its own, counteracting the magnetic field produced by the stator, inducing a voltage called rotor EMF, Electro-Motive Force. In the dynamic models, this is represented by the term  $j\omega_r\psi_R^s$ . Together with the voltage drop over the rotor, a voltage called back EMF,  $\mathbf{E}_b^s$ , is applied over the magnetizing inductance  $L_M$  in figure 2.4 [3].

$$\mathbf{E}_b^s = \left( j\omega_r - \frac{R_R}{L_M} \right) \psi_R^s \quad (2.6)$$

From figure 2.4 the voltage equations for the inverse- $\Gamma$  model can be derived:

$$\mathbf{v}_s^s - R_s \mathbf{i}_s^s - L_\sigma \frac{d\mathbf{i}_s^s}{dt} - L_M \frac{d\mathbf{i}_M^s}{dt} = 0 \quad (2.7)$$

$$j\omega_r \psi_R^s - R_R \mathbf{i}_R^s - L_M \frac{d\mathbf{i}_M^s}{dt} = 0 \quad (2.8)$$

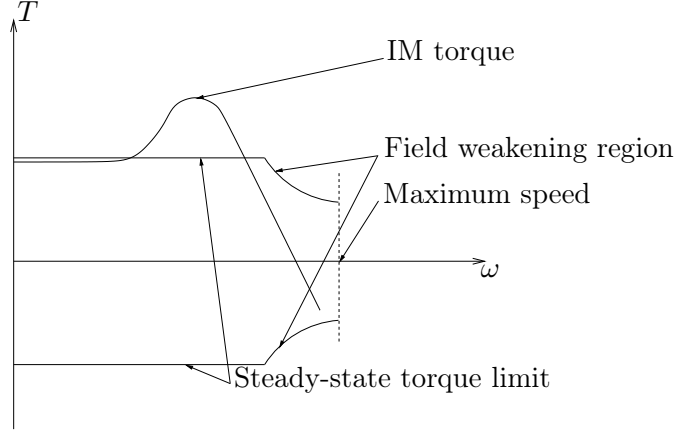


Figure 2.5: Comparison between IM-torque curves for a fixed stator frequency and for vector control with steady-state torque limit and maximum speed.

As the rotor currents are hard to measure, they are eliminated from equations (2.7) and (2.8) by introducing

$$\mathbf{i}_R^s = \mathbf{i}_M^s - \mathbf{i}_s^s = \frac{\psi_R^s}{L_M} - \mathbf{i}_s^s. \quad (2.9)$$

The voltage equations may now be written as

$$L_M \frac{d\mathbf{i}_s^s}{dt} = \mathbf{v}_s^s - R_s \mathbf{i}_s^s - \frac{d\psi_R^s}{dt} \quad (2.10)$$

$$\frac{d\psi_R^s}{dt} = R_s \mathbf{i}_s^s - \left( \frac{R_R}{L_M} - j\omega_r \right) \psi_R^s \quad (2.11)$$

Harnefors defines  $\frac{d\psi_R^s}{dt}$  as the flux EMF,  $\mathbf{E}^s$ . Comparing equation (2.6) with (2.11) it may be concluded that the difference at nominal speeds are small. Hence  $\mathbf{E}^s$  is often referred to as back EMF [3].

## Chapter 3

# Vector Control

The idea of vector control is to mathematically represent an AC machine as a DC machine [2]. Vector control relies on field orientation. In all rotating machines there is a magnetic field and if the control signals are aligned to this field, field orientated control is achieved.

### 3.1 Space Vectors

Space vectors were originally invented to describe spatial flux distributions in AC machines, hence “space” [2]. Due to the fact that  $v_a(t) + v_b(t) + v_c(t) = 0 \forall t$ , it is possible to describe the three-phase system as an equivalent two-phase system, with two perpendicular axes, with the axes denoted as  $\alpha$  and  $\beta$ . It is also convenient to think of these axes as the real and imaginary axes in a complex plane. The voltage vector in the complex plane is then denoted as  $\mathbf{v}^s(t) = v_\alpha(t) + jv_\beta(t)$ . The superscript “s” in  $\mathbf{v}^s$  means that the space vector is referred to the stator reference frame, meaning that the vector rotates with the stator speed which is zero.  $v_\alpha$  and  $v_\beta$  are calculated using the following transformation matrix

$$\begin{bmatrix} v_\alpha \\ v_\beta \end{bmatrix} = K \underbrace{\begin{bmatrix} \frac{2}{3} & -\frac{1}{3} & -\frac{1}{3} \\ 0 & \frac{1}{\sqrt{3}} & -\frac{1}{\sqrt{3}} \end{bmatrix}}_{T_{32}} \begin{bmatrix} v_a(t) \\ v_b(t) \\ v_c(t) \end{bmatrix} \quad (3.1)$$

where  $K$  is a scaling factor:

$$\begin{array}{ll} \text{Peak-value/Amplitude-invariant scaling:} & K = 1 \\ \text{RMS-value scaling:} & K = 1/\sqrt{2} \\ \text{Power-invariant scaling:} & K = \sqrt{3/2}. \end{array}$$

The inverse matrix of  $T_{32}$ ,  $T_{23}$ , is used to get from two-phase back to three-phase [2]

$$\begin{bmatrix} v_a(t) \\ v_b(t) \\ v_c(t) \end{bmatrix} = \frac{1}{K} \underbrace{\begin{bmatrix} 1 & 0 \\ -\frac{1}{2} & \frac{\sqrt{3}}{2} \\ -\frac{1}{2} & -\frac{\sqrt{3}}{2} \end{bmatrix}}_{T_{23}} \begin{bmatrix} v_\alpha \\ v_\beta \end{bmatrix}. \quad (3.2)$$

### 3.2 Synchronous Coordinates

The purpose of vector control is, as mentioned earlier, to control the AC machine as if it were a DC machine. If this is to be done, the control signals need to be DC quantities. This is achieved by the transformation from two-phase to synchronous reference frame,  $\mathbf{v} = e^{-j\omega_1 t} \mathbf{v}^s$  where  $\omega_1$  is the synchronous frequency. As the reference frame rotates with the supply/synchronous frequency, the vector appears not to be moving. This is called dq-transformation and its relations with  $\alpha$  and  $\beta$  leads to the following transformation matrix [2]

$$\begin{aligned} \mathbf{v} &= e^{-j\omega_1 t} \mathbf{v}^s = e^{-j\theta_1} \mathbf{v}^s = (\cos \theta_1 - j \sin \theta_1) (v_\alpha + jv_\beta) \\ &= v_\alpha \cos \theta_1 + v_\beta \sin \theta_1 + j(-v_\alpha \sin \theta_1 + v_\beta \cos \theta_1) \\ \Leftrightarrow \mathbf{v} &= \begin{bmatrix} v_d \\ v_q \end{bmatrix} = \underbrace{\begin{bmatrix} \cos \theta_1 & \sin \theta_1 \\ -\sin \theta_1 & \cos \theta_1 \end{bmatrix}}_{T_{dq}(\theta_1)} \begin{bmatrix} v_\alpha \\ v_\beta \end{bmatrix}. \end{aligned} \quad (3.3)$$

### 3.3 Motor Control

Vector control implies *rotor flux orientation*. Rotor flux orientation means that the rotor flux is aligned with the d-axis. The result is that the q-part of the rotor flux is zero.

Most significant for applying vector control is the measuring of the stator currents,  $\mathbf{i}_s$ , which are transformed to the equivalent two phase system,  $\alpha\beta$ . They are then dq transformed for the control system using the rotor flux oriented angle,  $\theta_1$  [2]. The rotor flux oriented angle is derived from the measured rotor speed  $\omega_r$  together with the calculated slip speed. The control system also provides the desired dq-frame stator voltage vector,  $\mathbf{V}_s$ , which in turn is  $\alpha\beta$ - and then two-phase/three-phase -transformed before it is amplified and fed to the IM, see Figure 3.1.

### 3.4 Sensorless Motor Control

As mentioned earlier, the traditional way of controlling an IM often involves a shaft sensor that measures the speed/position of the rotor. This sensor is costly, for low- and medium-powered drives it often matches the cost of the

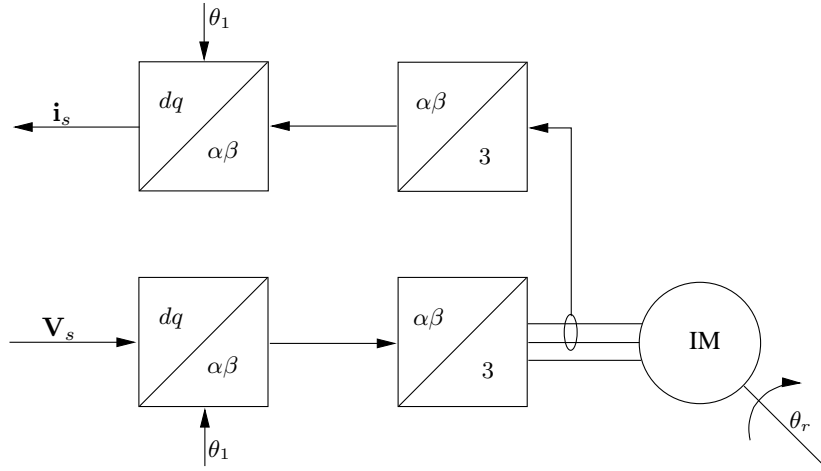


Figure 3.1: The idea of the vector control method, where the control system gets a voltage reference signal and then produces a three phase voltage to the IM. The rotor speed  $\omega_r$  is measured and added to a calculated slip speed, creating the synchronous speed  $\omega_1$ . This speed is then used to get the synchronous angle  $\theta_1$  necessary for the transformations from control signals to a three-phase voltage.

motor itself [2]. Besides the cost of the sensor it is also “one more part” that may fail. It is also possible to use a flux sensor but the usage of such kind of device is highly impractical due to probe placing between the stator and rotor.

Harnefors [2] distinguishes between three different types of sensorless control cases:

1. **Flux-sensored, speed-sensorless control:** When using a flux sensor, vector control is no more difficult than controlling a DC motor. An extra sensor for speed measurement is not needed because the speed can be calculated using slip subtraction.
2. **Flux-sensorless, speed sensed control:** The typical situation in most IM drives. Speed measuring allows design of flux estimators which give good performance at all speeds.
3. **Flux- and speed-sensorless control:** Estimates both the flux and speed which is an attractive solution due to reduced costs and parts. At nominal speeds, a flux-angle estimate of good accuracy can be obtained but they tend to fail when load torque is applied at very low speeds.

While for 1. and 2., stable operation is possible at all speeds, there is not yet proof of a flux- and speed-sensorless control that is able to function

## A Sensorless Induction Machine Drive.

---

completely stable at low frequencies while subjected to a load torque. The flux and speed-sensorless control is the focus of this thesis.

## Chapter 4

# Sensorless Control Algorithm

Several sensorless control strategies has been proposed. Anders Ottergren evaluated three different speed sensorless observers at Aros electronics AB in 2002: Observer based on Current-Voltage model (OCV), Adaptive Speed Observer (ASO) and Voltage Model with Indirect Field Orientation (VMIFO). Ottergren concluded that ASO was the preferred method [1].

Since Ottergrens work, the voltage model variants have improved. Lennart Harnefors describes a sensorless flux estimator called the Statically Compensated Voltage Model (SCVM) [2] first proposed in [6]. This method has been further developed by Rolf Ottersten [7]. In this thesis the improved SCVM is studied and implemented.

The estimators may be of two types, *Direct Field Orientation* (DFO) and *Indirect Field Orientation* (IFO). DFO estimate the flux space vector directly while IFO use the estimated rotor position to get the flux.

### 4.1 Improved Statically Compensated Voltage Model

The SCVM is based upon the classic "Voltage Model (VM)" flux estimator, derived from the relation

$$\frac{d\hat{\psi}_R^s}{dt} = \mathbf{E}^s. \quad (4.1)$$

This implies that if the flux EMF is known, the rotor flux may be found. Harnefors [2] deducts the SCVM quite thoroughly and this thesis only cover it briefly.

After transferring the VM from DFO to IFO representation and splitting the relation into real and imaginary parts, the following equations are obtained [7]:

$$\frac{d\hat{\Psi}_R}{dt} = E_d \quad (4.2)$$

$$\hat{\omega}_1 = \frac{E_q}{\hat{\Psi}_R} \quad (4.3)$$

where

$$E_d = v_d - R_s i_d + \hat{\omega}_1 L_\sigma i_q \quad (4.4)$$

and

$$E_q = v_q - R_s i_q - \hat{\omega}_1 L_\sigma i_d. \quad (4.5)$$

The VM achieves good results at nominal speeds, but low speed estimation is problematic. One common improvement is to replace the integrator needed to calculate  $\hat{\psi}_R^s$  with a low-pass integrator. Unfortunately, doing so adds a static error, equal at all frequencies. The error may be compensated for if a complex valued gain factor is introduced in the filter. This modified VM is called the Statically Compensated Voltage Model, or SCVM [2]. The flux will then be

$$\hat{\psi}_R^s = \frac{j\hat{\omega}_1 + \lambda|\hat{\omega}_1|}{j\hat{\omega}_1(p + \lambda|\hat{\omega}_1|)} \mathbf{E}^s = \frac{1 - j\lambda \text{sign}(\hat{\omega}_1)}{p + \lambda|\hat{\omega}_1|} \mathbf{E}^s \quad (4.6)$$

where  $p = \frac{d}{dt}$  and  $\lambda$  is a gain parameter greater than zero. Equation (4.6) may be transformed to IFO by substituting  $p \rightarrow p + j\hat{\omega}_1$  and  $\mathbf{E} \rightarrow E_d + jE_q$  and removing superscript "s". Splitting the result into real and imaginary parts and solving the imaginary part for  $\hat{\omega}_1$  gives

$$\hat{\psi}_R = \frac{E_d + \lambda \text{sign}(\hat{\omega}_1) E_q}{p + \lambda|\hat{\omega}_1|} \quad (4.7)$$

$$\hat{\omega}_1 = \frac{E_q - \lambda \text{sign}(\hat{\omega}_1) E_d}{\hat{\psi}_R} \quad (4.8)$$

Ottersten [7] then modifies the SCVM by introducing a new coefficient,  $\mu$ . By doing so, Ottersten adds another degree of freedom to the model.

$$\hat{\psi}_R = \frac{\mu E_d + \lambda \text{sign}(\hat{\omega}_1) E_q}{p + \lambda|\hat{\omega}_1|} \quad (4.9)$$

$$\hat{\omega}_1 = \frac{E_q - \lambda \text{sign}(\hat{\omega}_1) E_d}{\hat{\psi}_R} \quad (4.10)$$

## 4.2 Parameter Sensitivity of the SCVM

A crucial measure of the performance of a sensorless control algorithm is the sensitivity to variations in motor parameters. As the motor operates, the parameters may change substantially. The resistances are mainly affected by heat development and inductances by the level of magnetization and saturation. As a result, the most likely deviations will be increasing resistance and inductance. Other deviations may also occur, for example if parameters are wrongly measured or the motors differs in the production line.

Four parameters are included in the inverse- $\Gamma$  model; stator resistance  $R_s$ , rotor resistance  $R_R$ , magnetizing inductance  $L_M$  and total leakage inductance  $L_\sigma$ . In this project,  $L_\sigma$  is derived from the T-model parameters  $L_s$ ,  $L_r$  and  $L_m$ .

The SCVM includes three of the inverse- $\Gamma$  parameters,  $R_s$ ,  $R_R$  and  $L_\sigma$ . Indirectly the magnetizing inductance will affect  $L_\sigma$  according to equation (2.1). It may be rewritten as

$$L_\sigma = L_{ls} + \underbrace{L_m \left(1 - \frac{1}{\frac{L_{lr}}{L_m} + 1}\right)}_{\substack{\rightarrow L_{lr}, \text{ as } L_m \rightarrow \infty \\ \rightarrow 0, \text{ as } L_m \rightarrow 0}}. \quad (4.11)$$

The calculated leakage inductance will hence be between  $L_{ls}$  and  $L_{ls} + L_{lr}$ . As long as the magnetizing inductance changes are moderate the effect on  $L_\sigma$  will be small.

The critical parameter for the SCVM is the stator resistance [3]. It is used in the calculations of  $E_d$  and  $E_q$  and impact the calculated flux directly. The rotor resistance affect the slip calculation, thus affecting the accuracy of the drive to some extent. The total leakage inductance is a part of the flux estimation.

## 4.3 Known Limitations of the SCVM

The main problem region for the SCVM is low speed operation and reversing the motor when subjected to a larger load. Theoretically, the estimator is stable for all operating conditions except  $\omega_1 = 0$  and reversal with  $i_q > \frac{i_d}{\sqrt{2}}$  [2]. In practice, the low speed region where the SCVM is unstable is larger. Reversing with load is a problem mainly when doing so slowly. If the transition is fast, the probability of the problem developing is less. It is also dependent upon how accurately the stator resistance is modelled. Rolf Ottersten [7] suggest two improvements to make the SCVM more stable at reversal and low speed operation. The stator resistance may be modeled differently if  $\omega_1$  and  $i_q$  have the same sign or not, slightly underestimated in the first case and overestimated in the second. This requires the stator

resistance to be fairly well known. Ottersten also suggest a modification of  $\lambda$  at low speeds, choosing lambda to be

$$\lambda = \frac{\sqrt{2}|\omega_1|}{\omega_{1,min}} + \lambda_p(\hat{\psi}_R - \psi_{ref}) \quad (4.12)$$

where

$$\lambda_p = 3 \frac{|i_q|}{i_d}. \quad (4.13)$$

The success of the latter method depends upon that  $R_s$  is estimated in the manner described above. This approach is not yet fully tested. It is shown that with  $\lambda_p = 0$ , this method is an improvement at lower speeds.  $w_{1,min}$  is suggested to be between 5 and 10 % of nominal speed.

In this thesis, Otterstens improvements are not used.

## Chapter 5

# Simulations

Before proceeding with the implementation it is necessary to do some simulations in order to test the control strategy. It is also an opportunity to get acquainted with different problems that might arise during the implementation.

### 5.1 Motor Model

In this section, the mathematical model of the motor and its implementation in Matlab Simulink is described and constructed. The base for the motor model is the arbitrary dynamic model of an induction machine [5]:

$$\begin{bmatrix} v_{qs}^c \\ v_{ds}^c \\ v_{qr}^c \\ v_{dr}^c \end{bmatrix} = \begin{bmatrix} R_s + L_s p & \omega_c L_s & L_m p & \omega_c L_m \\ -\omega_c L_s & R_s + L_s p & -\omega_c L_m & L_m p \\ L_m p & (\omega_c - \omega_r) L_m & R_r + L_r p & (\omega_c - \omega_r) L_r \\ -(\omega_c - \omega_r) L_m & L_m p & -(\omega_c - \omega_r) L_r & R_r + L_r p \end{bmatrix} \begin{bmatrix} i_{qs}^c \\ i_{ds}^c \\ i_{qr}^c \\ i_{dr}^c \end{bmatrix} \quad (5.1)$$

where  $p = \frac{d}{dt}$ . The super- and subscript "c" denotes that the parameter should be replaced by the parameter specific for the reference frame chosen. If the reference frame is aligned with the rotor flux, the system is called synchronous and  $\omega_c$  is replaced with  $\omega_1$ . In this thesis, the motor is modeled with stationary references and  $\omega_c$  is replaced with 0. With stationary references, it is common to say that the model is an  $\alpha\beta$ -system where  $\alpha$  is aligned to the magnetizing d-axis ( $q = \beta, d = \alpha$ ). The rotor windings are short-circuited, leading to zero rotor voltage ( $v_{\beta r} = v_{\alpha r} = 0$ ), yielding

$$\begin{bmatrix} v_{\beta s}^s \\ v_{\alpha s}^s \\ 0 \\ 0 \end{bmatrix} = \begin{bmatrix} R_s + L_s p & 0 & L_m p & 0 \\ 0 & R_s + L_s p & 0 & L_m p \\ L_m p & -\omega_r L_m & R_r + L_r p & -\omega_r L_r \\ \omega_r L_m & L_m p & \omega_r L_r & R_r + L_r p \end{bmatrix} \begin{bmatrix} i_{\beta s}^r \\ i_{\alpha s}^r \\ i_{\beta r}^r \\ i_{\alpha r}^r \end{bmatrix}. \quad (5.2)$$

The flux linkages are defined as

$$\lambda_{\beta s} = L_s i_{\beta s} + L_m i_{\beta r} \quad (5.3)$$

$$\lambda_{\alpha s} = L_s i_{\alpha s} + L_m i_{\alpha r} \quad (5.4)$$

$$\lambda_{\beta r} = L_m i_{\beta s} + L_r i_{\beta r} \quad (5.5)$$

$$\lambda_{\alpha r} = L_m i_{\alpha s} + L_r i_{\alpha r}. \quad (5.6)$$

Rearranging (5.2) and inserting (5.3) - (5.6) and the differentiation of the same equations yields the differential equations implemented in the model of the motor. The goal with the transformations of the equations is to base the model on rotor flux and stator currents:

$$\frac{di_{\beta s}}{dt} = \frac{1}{L_s - \frac{L_m^2}{L_r}} \left( V_{\beta s} - R_s i_{\beta s} - \frac{L_m}{L_r} \frac{d\lambda_{\beta r}}{dt} \right) \quad (5.7)$$

$$\frac{di_{\alpha s}}{dt} = \frac{1}{L_s - \frac{L_m^2}{L_r}} \left( V_{\alpha s} - R_s i_{\alpha s} - \frac{L_m}{L_r} \frac{d\lambda_{\alpha r}}{dt} \right) \quad (5.8)$$

$$\frac{d\lambda_{\beta r}}{dt} = \omega_r \lambda_{\alpha r} - \frac{R_r}{L_r} \lambda_{\beta r} + \frac{L_m}{L_r} R_r i_{\beta s} \quad (5.9)$$

$$\frac{d\lambda_{\alpha r}}{dt} = -\omega_r \lambda_{\beta r} - \frac{R_r}{L_r} \lambda_{\alpha r} + \frac{L_m}{L_r} R_r i_{\alpha s}. \quad (5.10)$$

Further on, the flux and current index r and s will be omitted. The electrical torque produced is calculated using  $i_\alpha$ ,  $i_\beta$ ,  $\lambda_\alpha$  and  $\lambda_\beta$ .

$$T_e = \frac{n_p}{2} (i_\beta \lambda_\alpha - i_\alpha \lambda_\beta) \quad (5.11)$$

where  $n_p$  is the pole pair number. The mechanical part of the motor is represented by

$$T_e - T_L = J \frac{d\omega_r}{dt} + B\omega_r \quad (5.12)$$

where J is the moment of inertia and B is the viscous friction. Solving the equation for  $\omega_r$  gives

$$\omega_r = \frac{(T_e - T_L)}{J} e^{-Bt/J}. \quad (5.13)$$

Equations (5.7) - (5.13) are implemented in the “IM block” in Matlab Simulink together with the control system and transformation equations (3.1) - (3.3) as can be seen in figure 5.1. The motor parameters in the model are measured on the motor used in the implementation later on. The motor parameters can be found in Appendix A.

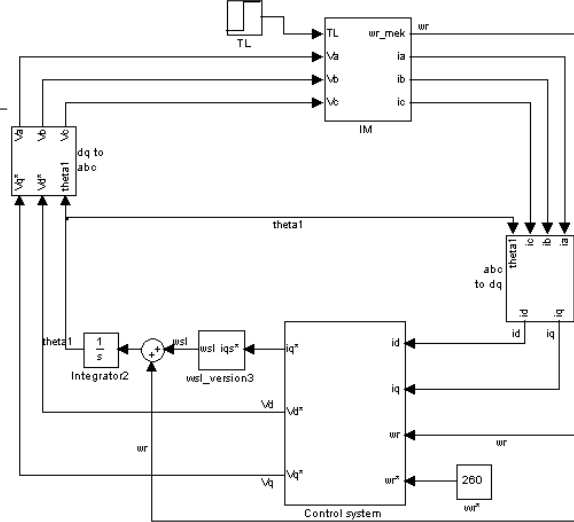


Figure 5.1: Simulink implementation of the motor and its controller using feedback of rotor speed.

## 5.2 Model Verification

Before beginning the sensorless implementation the model of the motor in figure 5.1 needs to be verified. In order to verify the motor model the outputs are compared to those of the real motor subjected to nominal speed and load torque, see figure 5.2. The phase voltage supplied to the motor in figure 5.2 is  $230 \cdot \sqrt{\frac{2}{3}}$  V (delta connected motor) and the nominal load torque is 3.73 Nm according to equation (5.14).

$$\frac{\text{nominal shaft power}}{\text{nominal speed}} = \frac{1100}{2815 \cdot \frac{60}{2\pi}} \approx 3.73 \text{ Nm} \quad (5.14)$$

As can be seen in figure 5.3 the simulated motor speed is  $\sim 46.9$  Hz. This is very close to the speed of the real motor during nominal conditions. The currents in figure 5.4 are close to the nominal rms phase-current, 4.41 A, of the machine. The verification testing indicates that the implemented motor model is realistic.

## 5.3 Control System Model

In this thesis, the input to the control system is chosen to be a speed reference. The control system in figure 5.1 is written as an S-function in Matlab for a more easy conversion to C-code. The control system in the first, non sensorless, version consists of a speed controller, two current controllers and a voltage decoupler.

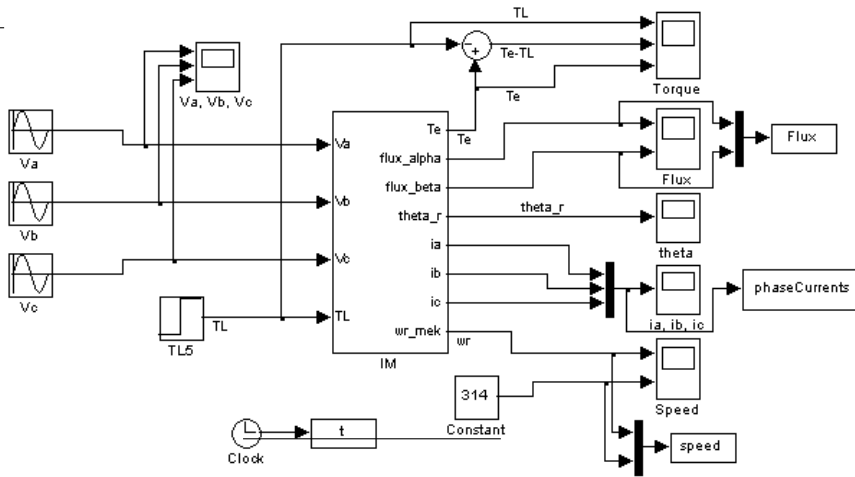


Figure 5.2: Verification of the implemented IM model.

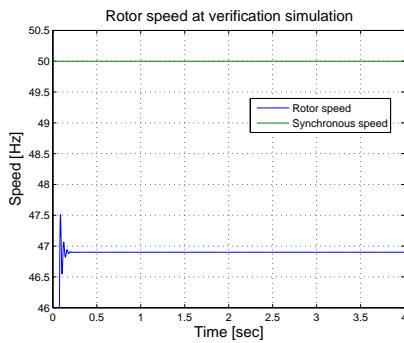


Figure 5.3: With the rotor speed at  $\sim 46.9$  Hz, the slip is  $\sim 6\%$  which is close to the real nominal slip, thus confirming the model.

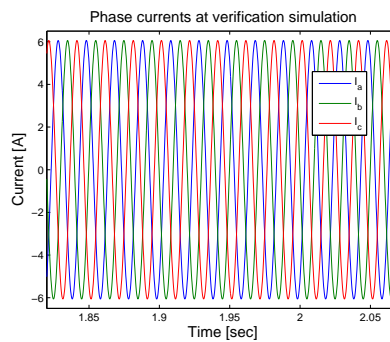


Figure 5.4: The peak-value of the currents are  $\sim 6$  A rendering the rms-value of 4.2 A, which is close to nominal current when the motor is cold.

The PI speed controller derives  $i_q^*$  from the speed error.

As discussed in Section 3.3,  $\lambda_{qr}^*$  is defined as zero. The  $\lambda_{dr}^*$  reference is set to a constant value [8]. From (5.9) the setpoint for  $i_{ds}$  is then

$$i_{ds}^* = \frac{\lambda_{dr}^*}{L_M} \quad (5.15)$$

Considering equation (5.15), the torque is proportional to  $i_{qs}^*$ . With the reference currents and the measured  $dq$  motor currents, the two current controllers are implemented. The output from these controllers are fed to a voltage decoupler, designed from the inverse  $\Gamma$ -model to remove the cross-coupling between d and q dependency while calculating the voltage commands to the "dq to abc" transformation block [3].

$$v_q^* = H_q + \hat{\omega}_1 L_\sigma i_d^* - (R_s + R_R) i_q^* \quad (5.16)$$

$$v_d^* = H_d - \hat{\omega}_1 L_\sigma i_q^* - (R_s + R_R) i_d^* \quad (5.17)$$

where  $H_q$  and  $H_d$  is the result from the current controllers.

## 5.4 The Improved SCVM Model

Lennart Harnefors describes a discrete improved SCVM algorithm that is implemented in this thesis project [2].

$$E_d = v_d^{ref} - R_s i_d^{ref} + \hat{\omega}_1 L_\sigma i_q^{ref} \quad (5.18)$$

$$E_q = v_q^{ref} - R_s i_q^{ref} - \hat{\omega}_1 L_\sigma i_d^{ref} \quad (5.19)$$

$$\hat{\psi}_R = \hat{\psi}_R + T_s \left( \mu E_d + \lambda \text{sign}(\hat{\omega}_1) E_q - \lambda |\hat{\omega}_1| \hat{\psi}_R \right) \quad (5.20)$$

$$\hat{\omega}_{slip} = R_R \frac{i_q^{ref}}{\hat{\psi}_R} \quad (5.21)$$

$$\hat{\omega}_r = \hat{\omega}_r + T_s \alpha_e \left( \frac{E_q - \lambda \text{sign}(\hat{\omega}_1) E_d}{\hat{\psi}_R} - \hat{\omega}_{slip} - \hat{\omega}_r \right) \quad (5.22)$$

Equation (5.18), (5.19) and (5.20) corresponds to equation (4.4), (4.5) and (4.9), respectively. Equation (5.21) is the standard slip relation. As the observant reader may notice, the calculation of  $\hat{\omega}_1$ , equation (4.10), is a part of the equation describing the rotor speed, (5.22). This is not a head on solution but a filter, making the estimate less sensitive to disturbances. This is possible as the mechanical system is slower than the control system.

The SCVM parameters is chosen as recommended by Harnefors,  $\mu = -1$  and  $\lambda = \sqrt{2}$ . The bandwidth  $\alpha_e$  of the rotor speed filter is set equal to the current controller bandwidth [2].

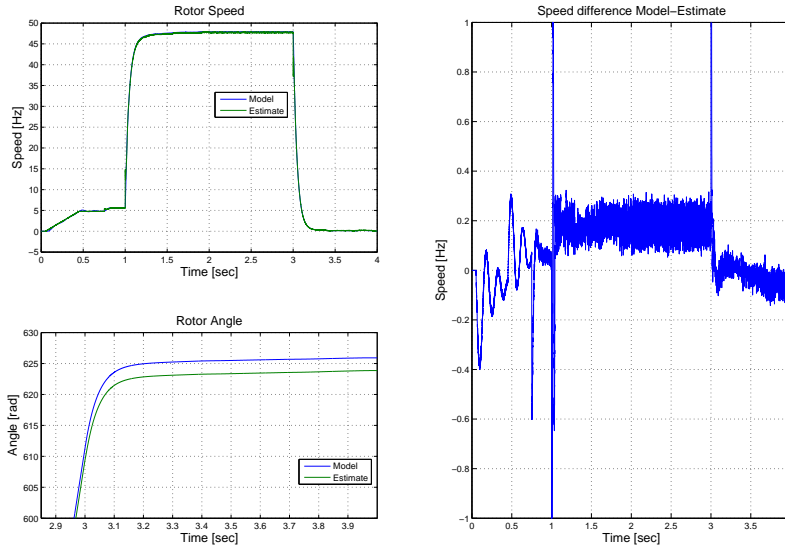


Figure 5.5: Modelled and estimated rotor data during an acceleration and retardation test, showing both speed, speed difference and angle when the motor is unloaded.

## 5.5 Simulation Results

To get some idea of the performance of the estimator, different scenarios are simulated.

Figure 5.5 shows some simulated and estimated rotor quantities during an acceleration and retardation of the motor. Figure 5.6 shows the same as figure 5.5 but the motor is subjected to a 2 Nm load. In both figures the top left image displays the speed of the rotor. The bottom left image shows the total angle of the rotor, and the speed difference between the estimation and the model are shown to the right. As may be seen in both figures, the angle difference after the test cycle is less than 1 %. The speed difference is also small, except for short periods when the speed command change instantaneously.

Section 4.3 states that a slow reversal of the induction machine may be problematic. To simulate such a case, a speed governed torque limited load model is developed. The load speed reference is set to a constant value while the motor speed command is varied as a saw-tooth signal. Two different cases are studied, one with step changes in load torque limitation, figure 5.8, and one with a constant load torque limit and also a deviation in the stator resistance value, figure 5.9. As seen in figure 5.8, the estimator can handle almost nominal load with slow ramping around zero excitation frequency.

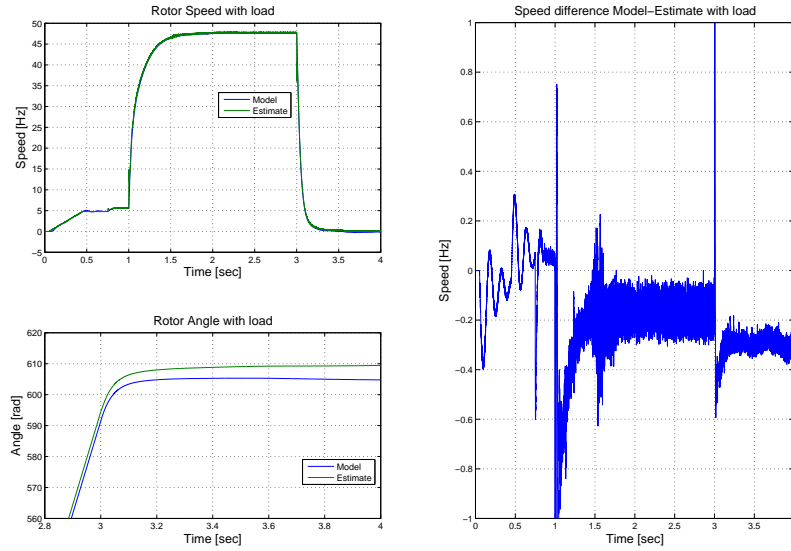


Figure 5.6: Modelled and estimated rotor data during an acceleration and retardation test, showing both speed, speed difference and angle with 2 Nm load.

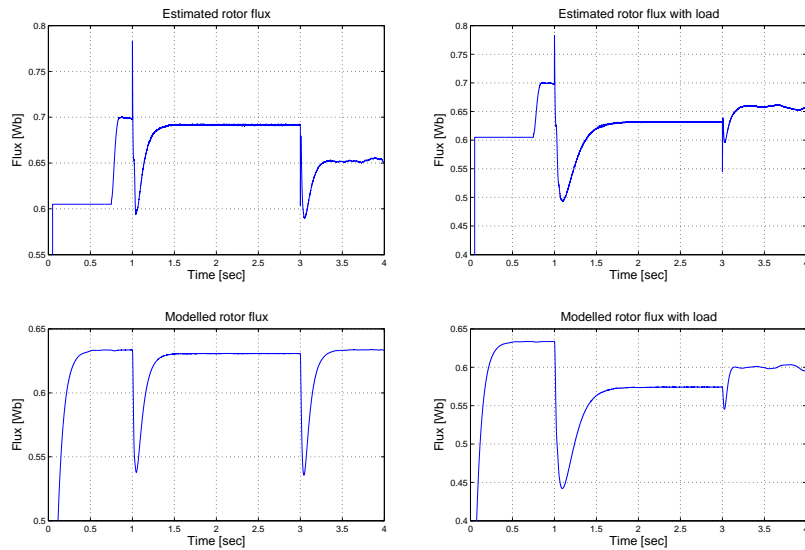


Figure 5.7: Modelled and estimated rotor flux during an acceleration and retardation with and without load.

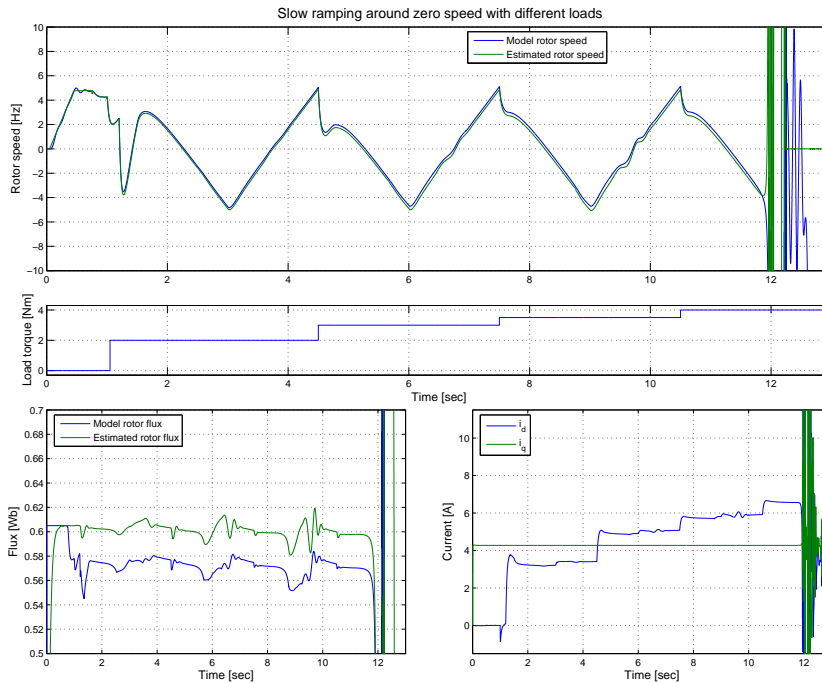


Figure 5.8: Simulated ramping around zero speed with stepwise increase of load torque.

The difference in estimated and modelled flux depend upon the different models used. The motor is implemented in the T model and the control system parameters are derived from the inverse- $\Gamma$  model and according to equation (2.4), the flux differs with the factor  $\frac{L_m}{L_r}$ . The ability to handle a deviation of the stator resistance in the motor is not good according to Figure 5.9. The flux will soon destabilize and the ability to follow the speed command will be reduced.

## 5.6 New Parameters

To optimize the usage of the MCU, the control system calculations are best done with integers. To accomplish this, all parameters in the control system is recalculated with suitable factors. These factors should be a power of two, as it is logical for the processor to work with. The factor for resistance is 256 ( $2^8$ ), for inductances it is 65536 ( $2^{16}$ ). Integer calculation with small values will render large errors (if the current is 1.49 A, the system will round it to 1 A). To avoid this, the control system is working with different units. The unit for current is 10 mA, voltage 10 mV and speed 10 mHz.

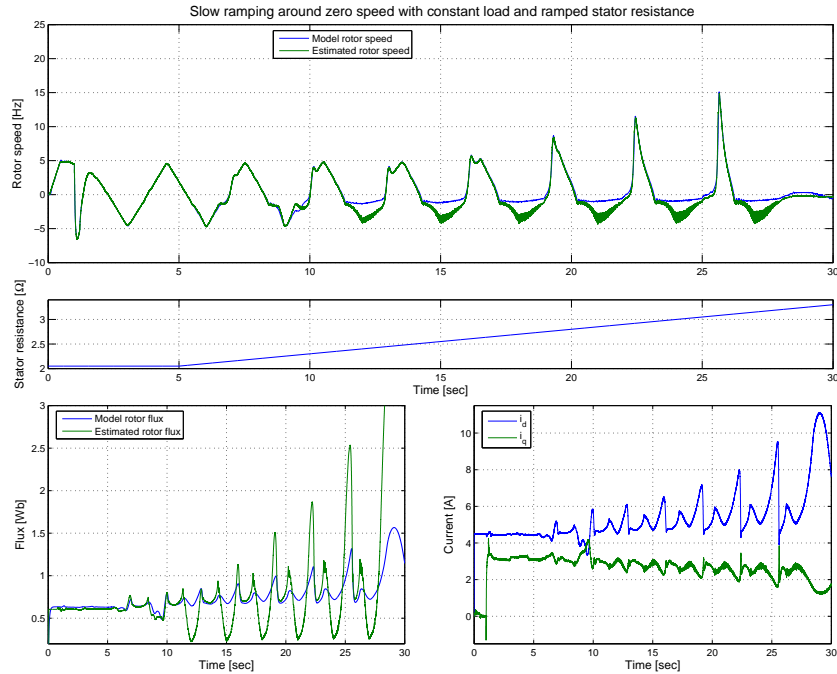


Figure 5.9: Simulated ramping around zero with constant load and ramped stator resistance.

## 5.7 Simulation Conclusions

The SCVM can handle static load, acceleration and deceleration. It also seem promising in reversing a speed governed load, at least if the motor parameters are modelled correctly. The quite high dependency of the stator resistance may be a problem, but all together it is worth to evaluate this approach experimentally.

## Chapter 6

# Implementation

A difficult feature of the control system when moving from simulations to implementation is that the DSP use 16-bit integer representation. This calls for a careful review of the implemented code. Any part of the computations exceeding 16-bit (+/- 32768 as most integers used are signed) has to be revised. It is also good if the code is optimized to use the DSP as effective as possible. Apart from estimator and control algorithms, there has to be capacity left for applications.

This chapter describes different parts of the implementation, beginning with hardware, continuing with software and data acquisition then ending with implementation issues.

### 6.1 Hardware

#### 6.1.1 Controller Card

This project uses a hardware setup constructed by Aros electronics AB. The controller card is a prototype from another project and is to large extent a standard converter-inverter design.

The board is prepared for using an encoder. In this project, the encoder is used as a reference for evaluation of the speed estimator. The encoder is capable of measuring speeds up to 50 Hz.

The communication with the computer during test and programming is operated by a serial interface. A special interface adapter is used to translate between the PC and the controller card. It is also equipped with optocouplers to galvanically isolate the two systems. The earth potential of the controller card may reach several hundreds of volts compared with the potential of the grid, thus harming the computer. The optocouplers transfer the signals from one voltage system to another.

The card has an on-board three phase diode bridge rectifier, a 36MT120 from International Rectifier. It is rated 35 A continuously and 1200 V peak

DC voltage. DC/DC converters use the main DC voltage to extract the power levels needed by the control card.

The phase currents are measured for the control system and for the over-current protection. If a too high current, about 40 A, is registered, a signal is sent to the processor and the system shuts down. The DC current is also measured, to if necessary invoke an over-current protection. The DC over-current trigger is set to 50 A. The control system also has to gain knowledge about the DC voltage. A voltage divider is connected to a voltage follower and read by an AD channel on the DSP.

### 6.1.2 Motor

The test motor is constructed by Bonfiglioli Group in Italy. The rated power is 1,1 kW and it has two poles. Motor data can be found in Appendix A.

## 6.2 Software

The software at Aros electronics AB is modular and the same modules appear in many of the company's products. One aim with this project is to develop an estimator that is easy to adapt to present and future projects at Aros. It should be enough to replace the encoder routine calls with the estimator ditto, adjust the parameters and the motor drive should be operational.

The estimator is only a small part of the controller software. In this thesis, a software package developed at Aros electronics AB is used. The basic control system already present is not altered. There are some differences between the simulated and the already implemented control system, the most important being that the speed controller use reference value filtering. It controls the speed in two levels, stepping the actual reference value toward the desired value. Reference value filtering allows a more stable controller. Another difference is the absence of a voltage decoupler in the control system.

To manipulate the system during test, a special PC-program is used. It is developed at Aros electronics AB. The software can control and monitor each variable in the DSP. It also has the possibility to display graphs of up to three variables at the same time.

## 6.3 Data Acquisition

There are three possibilities to access the parameters from the processor.

- The control PC-program has a logging feature including a graph tool. It is possible to log and graph three different signals through the serial control interface. Unfortunately, the sampling time of the system becomes large and erratic. For system supervising while running the motor it is adequate, but not for keeping track of transient behavior.

- Some projects at Aros have used MCU or on-board memory for logging data which is transferred to the computer as a file after the measurement. The equipment used in this project lacks the memory capacity needed for such approach.
- The board used is equipped with a Serial Peripheral Interface bus (SPI). SPI is a loose standard for serial communication. The idea with the interface in this project is to let the software use pins on the DSP to put out up to three signals to an external decoding circuit. The signals can then be studied using an oscilloscope. The sample rate is decided by how often the SPI code is executed in the DSP. In this project, the SPI call is located in the switch interrupt, rendering a sample rate equal to the switching frequency. The SPI has low amplitude resolution, 8 bits. The signal range is 0 to 3.68 V, a level sensitive to the harsh lab environment. While running the motor, the switched currents induce an electromagnetic field large enough to introduce noticeable disturbance when measuring the signals.

As described above, two methods are of interest in this case. The sampling time of the control PC-program is bad. On the other hand, the amplitude resolution of the SPI is narrow. In this thesis, the system is sampled via the SPI as it is assumed that the transient behavior is of more importance for evaluation of the SCVM than the amplitude resolution.

## 6.4 Implementation Issues

Going from simulation to the actual system proved to be troublesome. One large obstacle were the 16-bit limit for all variables. The calculations need to be large enough to get good accuracy (see Section 5.6), but sufficiently small to fit inside the 16-bit representation. Several adjustments had to be done to accomplish this. Some calculations were also split into several lines to get a better overview as well as making it easier for the compiler to interpret the code. There were some pure coding errors that took time to find. Even after careful review, some issues remained. For a final debug of the system, the implemented c-code was translated back to Matlab. The code was simulated bit by bit in the model used to develop the same. The errors were then quite easily found and corrected.

# Chapter 7

## Results

The implemented design is put through several tests to check the performance of the drive. It is of interest to see the operational limits concerning slow speed, parameter variation and transient behavior as well as speed stability up to twice the nominal load.

In order to get more information from the measurements, the measured data are filtered. The filter parameters are created using the `cheby2` function in Matlab with a cutoff frequency of 1500 Hz and stop-band attenuation of 110 dB.

### 7.1 Speed Step Response

Figures 7.1-7.4 depicts the step response as a speed change from zero to near nominal speed is applied to the control system. As may be seen, the drive is capable of handling different loads. The somewhat slower response for the double nominal load, figure 7.4, is a result from the current limit.

### 7.2 Slow Speed

The slow speed performance is tested by applying different loads and varying the speed command. The aim is to find the slow speed limit and the load limit at slow speed reversal of a speed governed load.

#### 7.2.1 Slow Speed Limit

In the first test, the load is set to -16 Hz and nominal torque, 3.7 Nm. The control system reference speed is programmed to decrease from 10 Hz to standstill with steps of 0.5 Hz. Figure 7.5 shows that it is possible to lower the speed and keep control of the motor, although the accuracy decrease.

In the second test, the reference speed is set to go from -10 Hz to zero. As may be seen in figure 7.6, the system fails already at 7.5 Hz. The test is

## A Sensorless Induction Machine Drive.

---

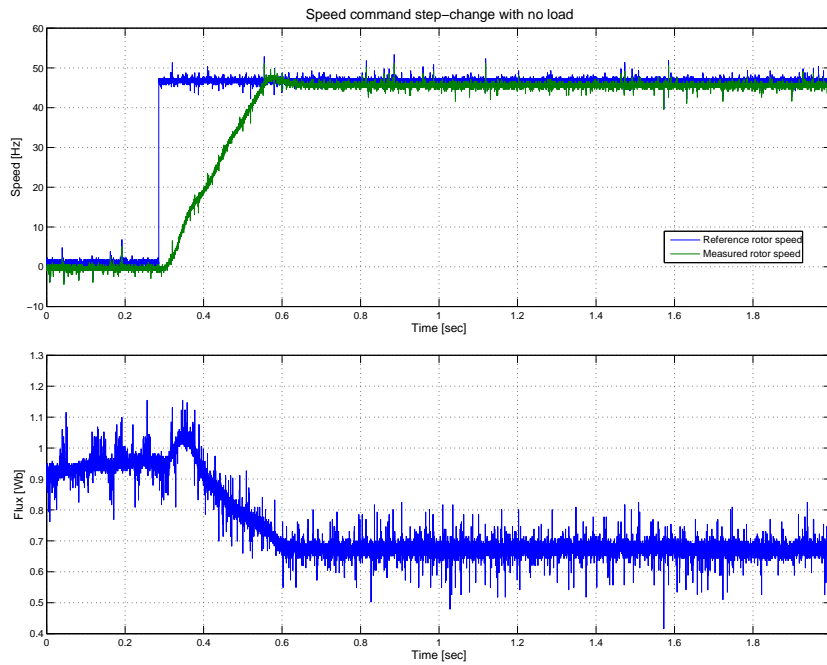


Figure 7.1: Speed step with with no load.

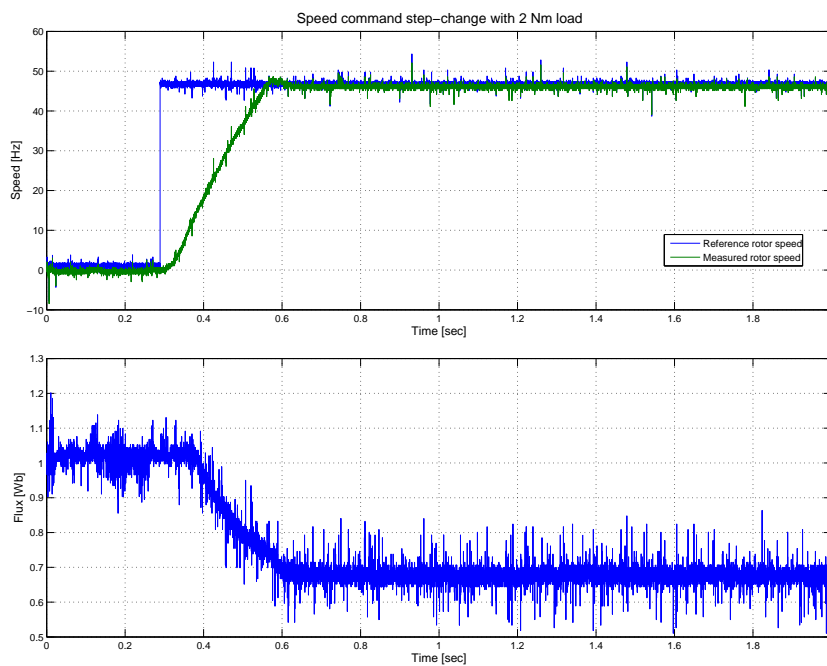


Figure 7.2: Speed step with 2 Nm load.

## A Sensorless Induction Machine Drive.

---

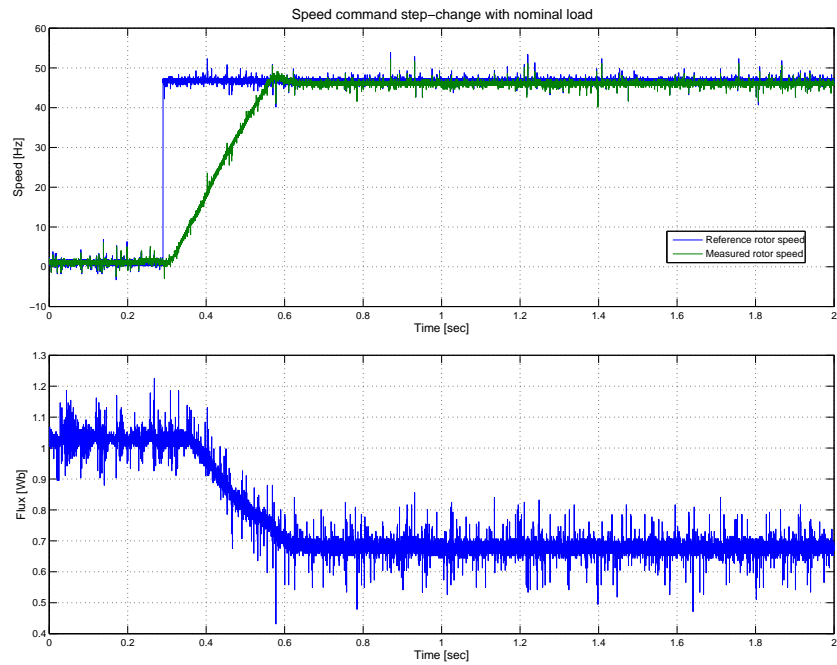


Figure 7.3: Speed step with nominal load, 3.7 Nm.

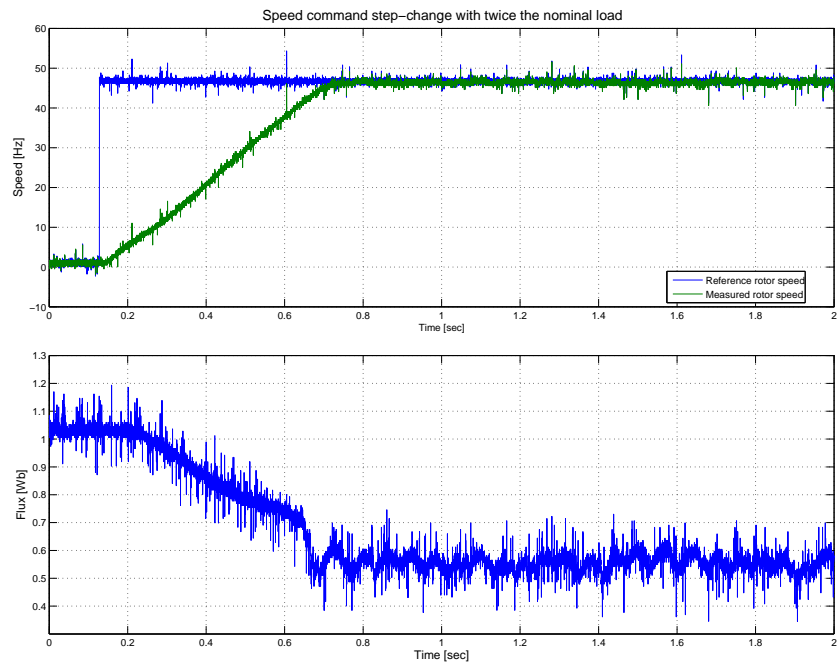


Figure 7.4: Speed step with double nominal load, 7.5 Nm.

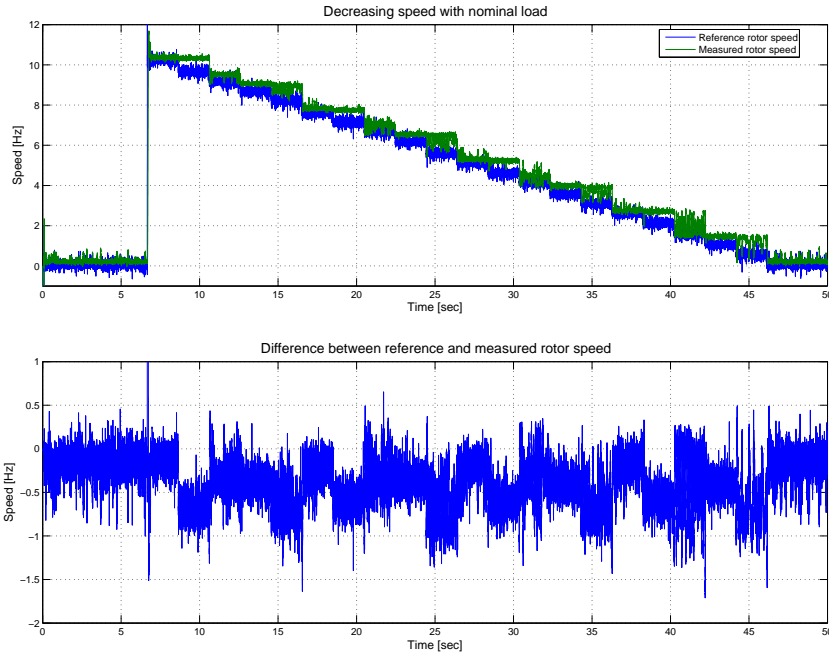


Figure 7.5: Decreasing speed with load and motor operating in the opposite direction. The load torque limit is set to motor nominal torque, 3.7 Nm.

redone with less load torque, 2 Nm. From the result in figure 7.7 it may be seen that the accuracy is significantly less compared to the test with positive movement, but the drive does not destabilize.

## 7.2.2 Reversing

The purpose is to test consequential slow reversals. As may be seen from figures 7.8-7.10, the load servo is controlled to a speed of -16 Hz. In all tests, the rotor is first operated at almost standstill. Keeping zero speed is difficult, in reality there is a small positive movement of the rotor. In figures 7.8 and 7.9, only the rotor speed, reference speed and estimated rotor speed is plotted. The drive is quite capable of handling reversal of such loads, but the transition is less smooth for 2 Nm. For a 3 Nm load, figure 7.10, the drive loses control but regains it once the speed is increased above zero. To enable an analysis of the occurring problem, the test is redone with logging of estimated rotor flux and measured stator currents.

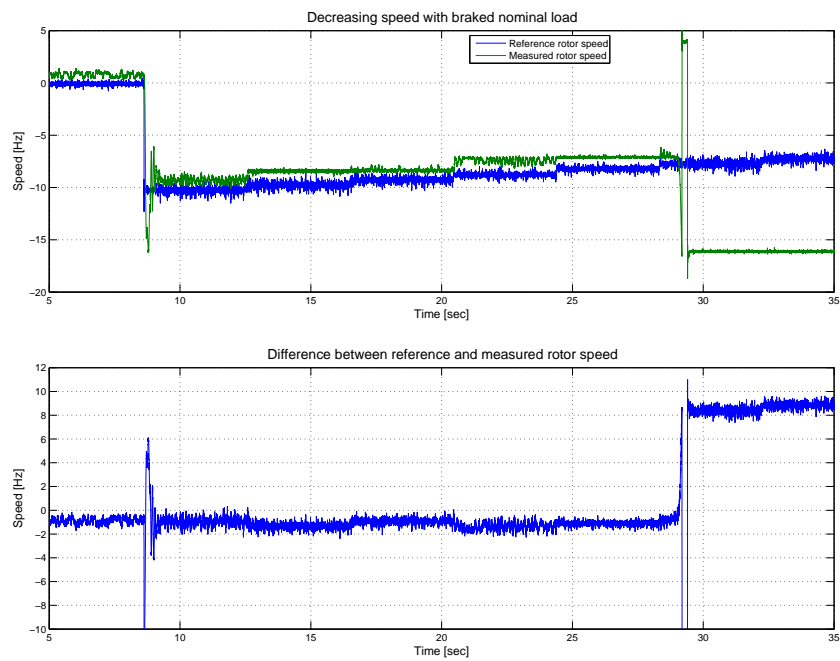


Figure 7.6: Decreasing speed with load and motor operating in the same direction, thus the motor tries to brake the load. The load torque limit is set to motor nominal torque, 3.7 Nm.

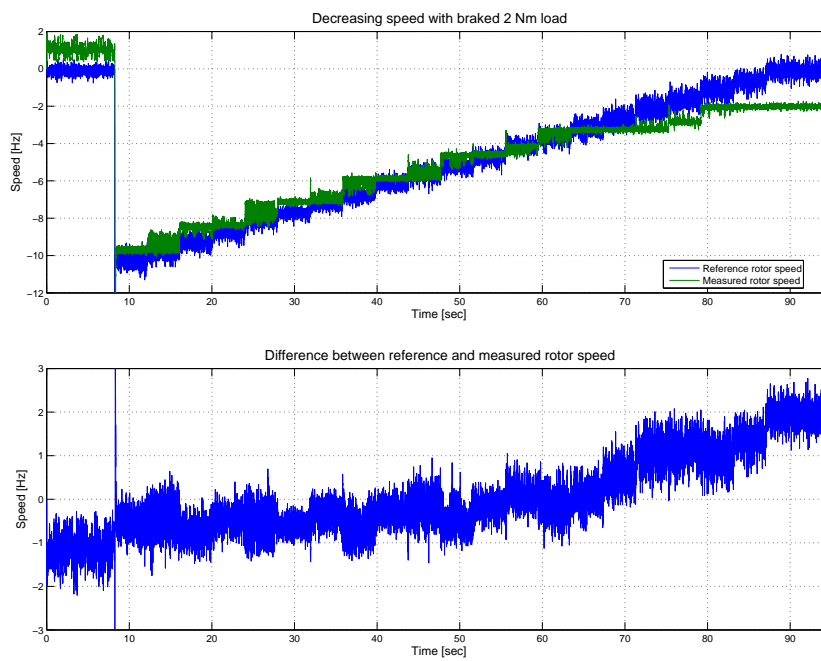


Figure 7.7: Decreasing speed with load and motor operating in the same direction, thus the motor tries to brake the load. The load torque limit is set to 2 Nm.

## A Sensorless Induction Machine Drive.

---

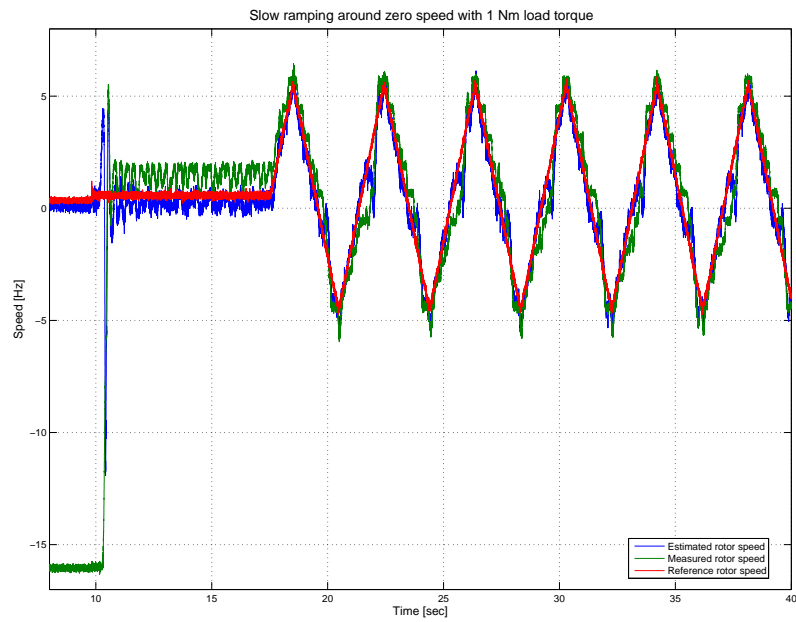


Figure 7.8: Slow ramping around zero speed with 1 Nm speed governed load.

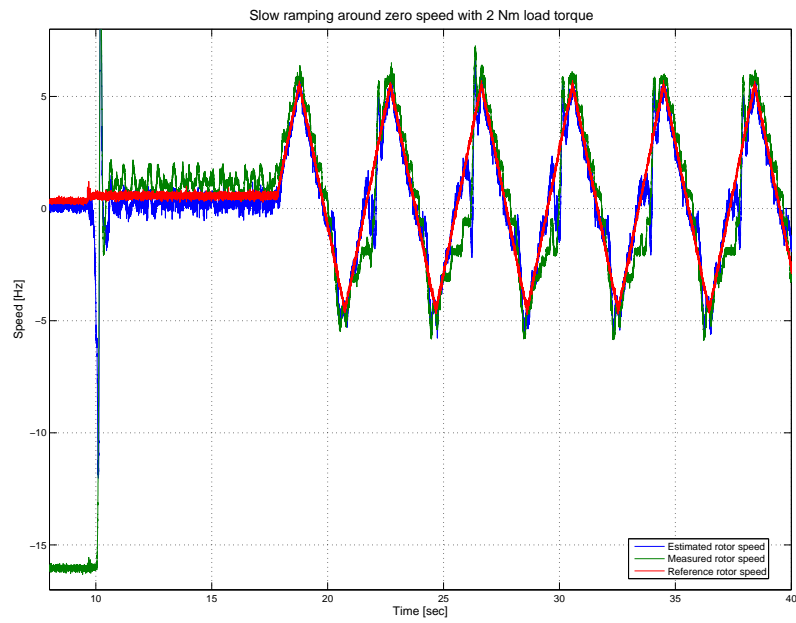


Figure 7.9: Slow ramping around zero speed with 2 Nm speed governed load.

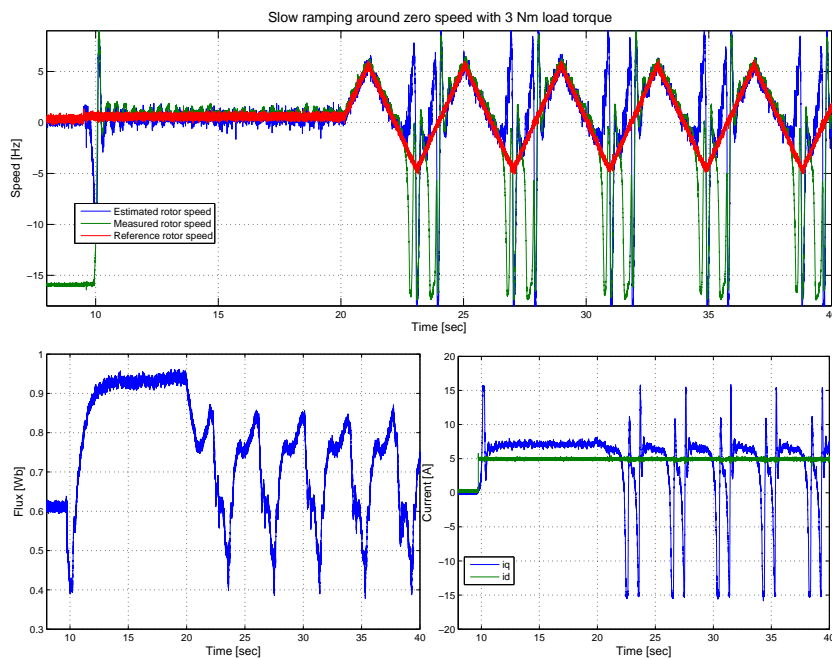


Figure 7.10: Slow ramping around zero speed with 3 Nm speed governed load. The two bottom plots are from a second test.

## 7.3 Parameter Sensitivity

To properly test the SCVMs ability to withstand parameter deviations, the motor parameters would need to be controllable. As this is hard to achieve, parameter changes are emulated by changing the parameter values in the implemented code. Doing so, the estimator will be subjected to similar stresses as if the real motor parameters were to change. The resistance values are changed to emulate a deviation of  $\pm 60\%$  and the leakage inductance to emulate  $\pm 30\%$ .

The motor is loaded with 2 Nm, as it seems to be able to handle it but with some difficulty, see figure 7.9. The aim with these tests is to find out how the performance at nominal speed and at low speed ramping about zero is affected by variations of stator and rotor resistance and leakage inductance.

### 7.3.1 Deviations in Stator Resistance

To test the estimators ability to cope with an increase in stator resistance,  $R_s$  is lowered in the control system. The test is conducted in two modes, slow ramping around zero with 2 Nm speed governed load, figure 7.11, and near the nominal speed with the same load, figure 7.12. The test is not conducted exactly at nominal speed as the encoder with its interface is unable to handle more than 50 Hz. Nominal rotor speed is 46.9 Hz, but with overshoot and other effects, it may be too large. Therefore, the rotor speed setpoint is 45 Hz. Each mode is tested twice, first to get encoder speed, estimated rotor speed and rotor resistance of the control system. In the second run, the estimated rotor flux and the measured, dq-transformed, currents are logged. This is due to the limitations of the SPI interface, see Section 6.3.

As seen in figure 7.11, the stability and accuracy reduce as the control system stator resistance is lowered. When the control system stator resistance is increased at low speed operation, figure 7.13, the drive fails. To see more exactly where this phenomena occurs, an even slower ramp is tested, see figure 7.14. From the graph it is found to happen at approximately 3.25  $\Omega$ . This corresponds to a motor stator resistance decrease by 37%. At higher speeds, a control system stator resistance change affect the drive insignificantly, as seen in Figures 7.12 and 7.15.

Especially in the low speed region, the SCVM is sensitive to inaccurately modeled stator resistance. However, it is not as bad as the simulations in Section 5.5 indicated. In the high speed region, the impact of the  $R_s i^s$  part in the equations (5.18) and (5.19) becomes less due to the increased importance of  $\hat{\omega}_1 L_\sigma i^s$ .

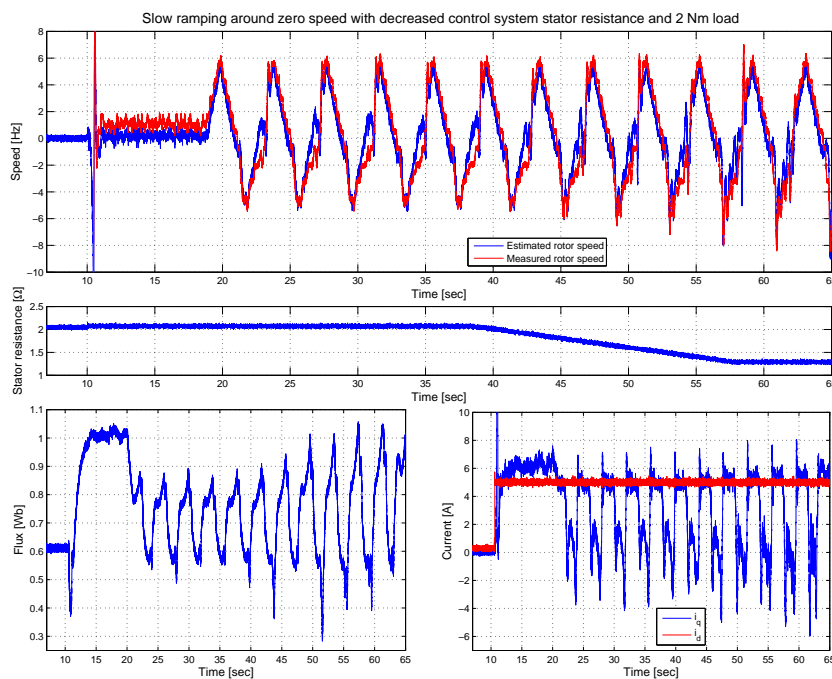


Figure 7.11: Speed, estimated rotor flux and measured currents at ramped speed around zero as the control system stator resistance is changed. A lower resistance means emulating an increase of motor stator resistance. The test is conducted twice, first to log speeds and resistance and secondly to log flux and currents.

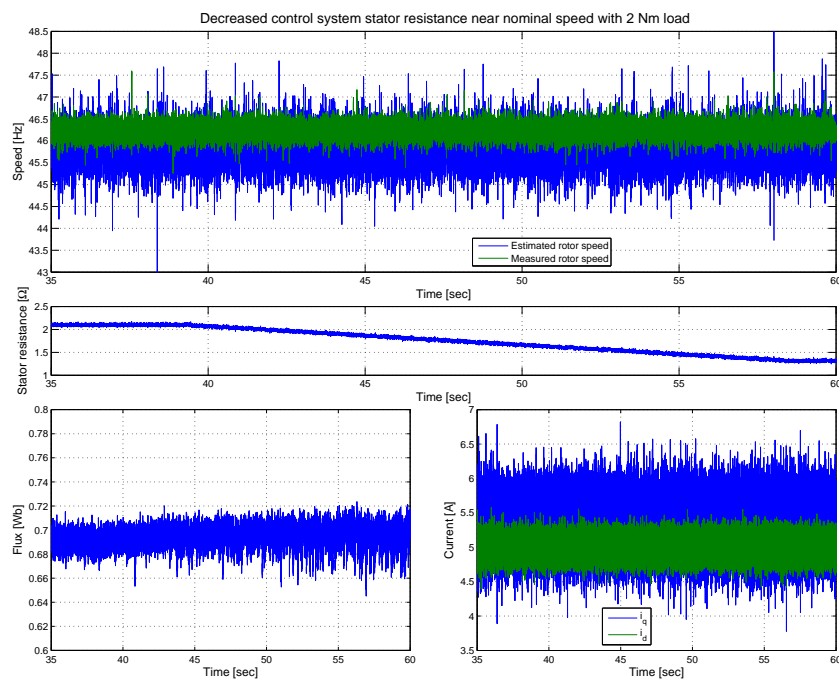


Figure 7.12: Speed, estimated flux and measured currents at near nominal speed as the control system stator resistance is changed. A lower resistance means emulating an increase of motor stator resistance. The test is conducted twice, first to log speeds and resistance and secondly to log flux and currents.

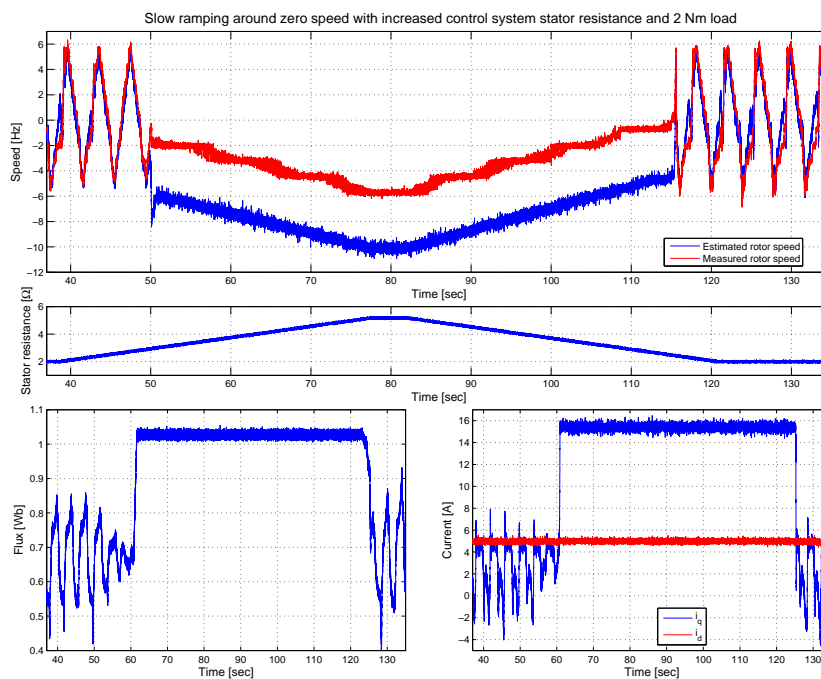


Figure 7.13: Speed, estimated flux and measured currents at ramped speed around zero as the control system stator resistance is increased. The test is conducted twice, first to log speeds and resistance and secondly to log flux and currents.

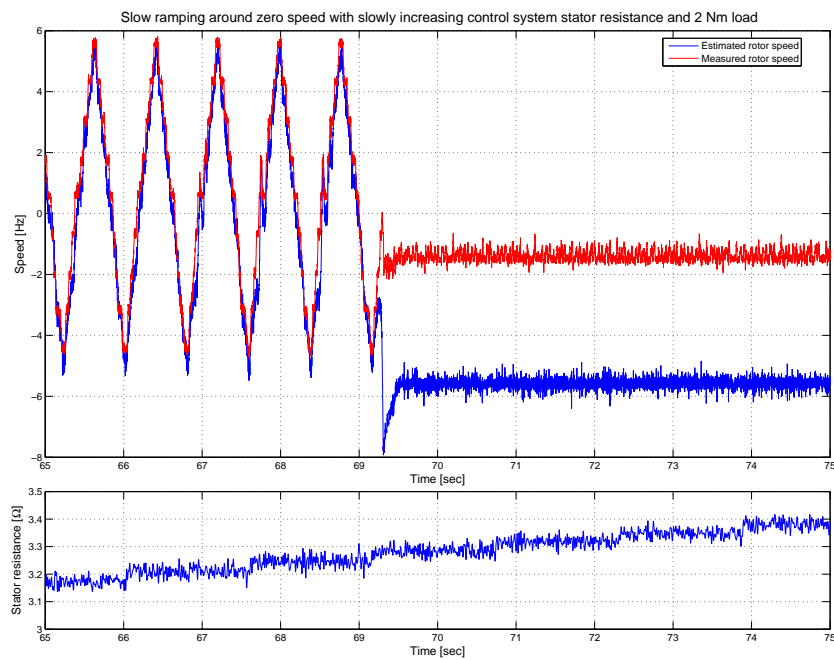


Figure 7.14: Estimated and measured speed as the control system stator resistance is slowly increased to see the troublesome resistance level.

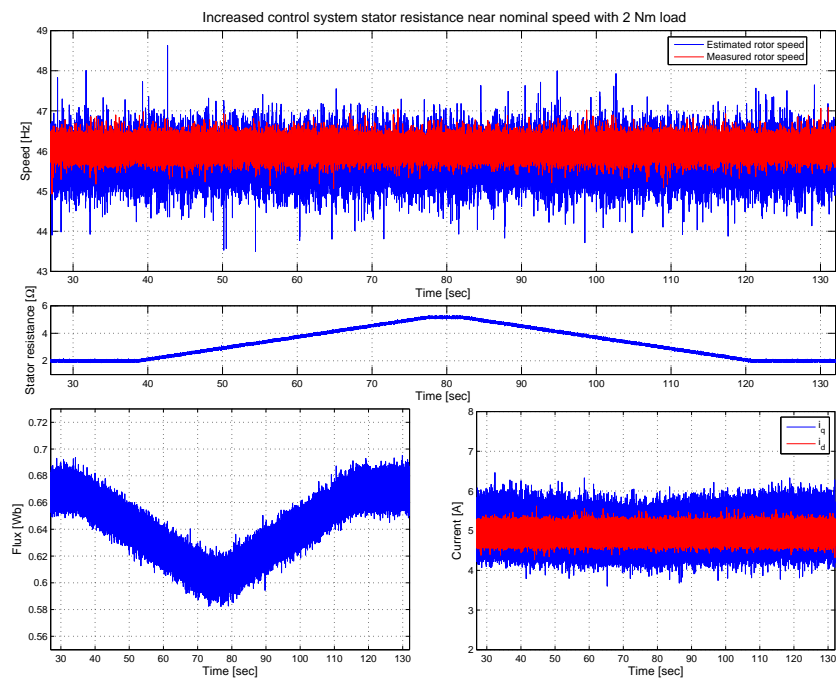


Figure 7.15: Speed, estimated flux and measured currents at near nominal speed as the control system stator resistance is first increased, then lowered to the nominal value. The test is conducted twice, first to log speeds and resistance and secondly to log flux and currents.

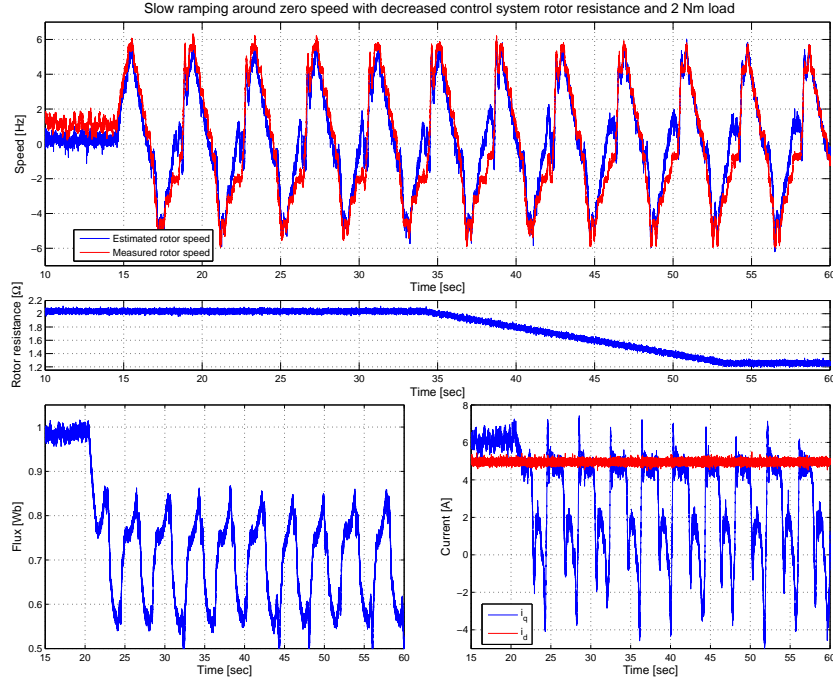


Figure 7.16: Speed, estimated rotor flux and measured currents at speed ramped about zero as the control system rotor resistance is changed. A lower resistance means emulating an increase of motor rotor resistance. The test is conducted twice, first to log speeds and resistance and secondly to log flux and currents.

### 7.3.2 Deviations in Rotor Resistance

The rotor resistance affects the slip calculation. The tests are conducted in the same way as for the stator resistance. As it may be seen in figure 7.16, the low speed operation of the SCVM hardly change at all with a decrease in control system rotor resistance. Figures 7.17 and 7.19 on the other hand depicts that in nominal or high speed region, the impact on the accuracy is more significant. As the control system rotor resistance is decrease in figure 7.17, the measured rotor speed decrease approximately 2 %. If the motor rotor resistance decrease much, the drive will even destabilize. At low speed, figure 7.18, the speed oscillation starts when the motor rotor speed is emulated to have decreased with 58 %. At near nominal speed, figure 7.19, the drive destabilize at 53 %.

Equation (5.21) models a linear relation between rotor resistance and slip speed. The slip is small at low speeds.

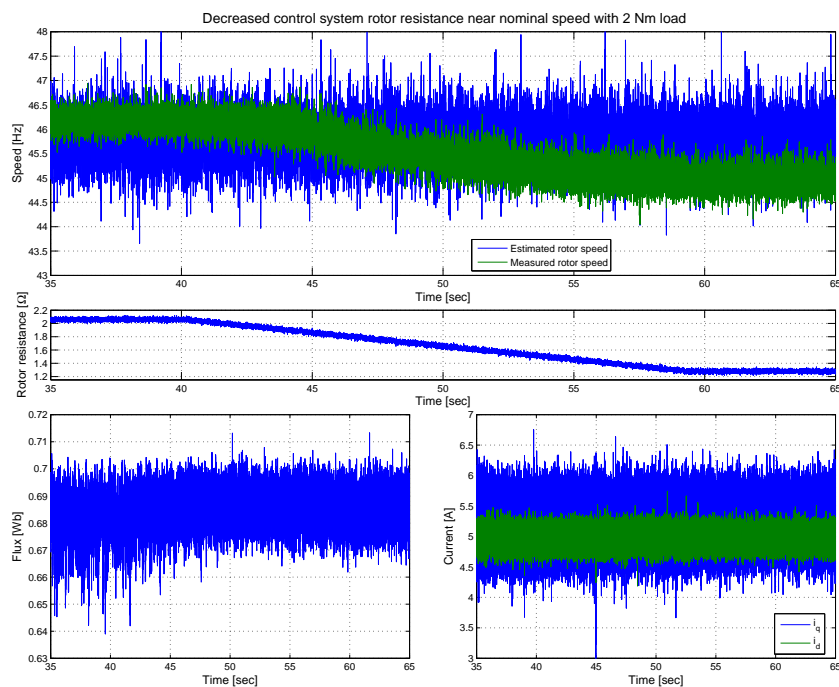


Figure 7.17: Speed, estimated rotor flux and measured currents at near nominal speed as the control system rotor resistance is changed. A lower resistance means emulating an increase of motor stator resistance. The test is conducted twice, first to log speeds and resistance and secondly to log flux and currents.

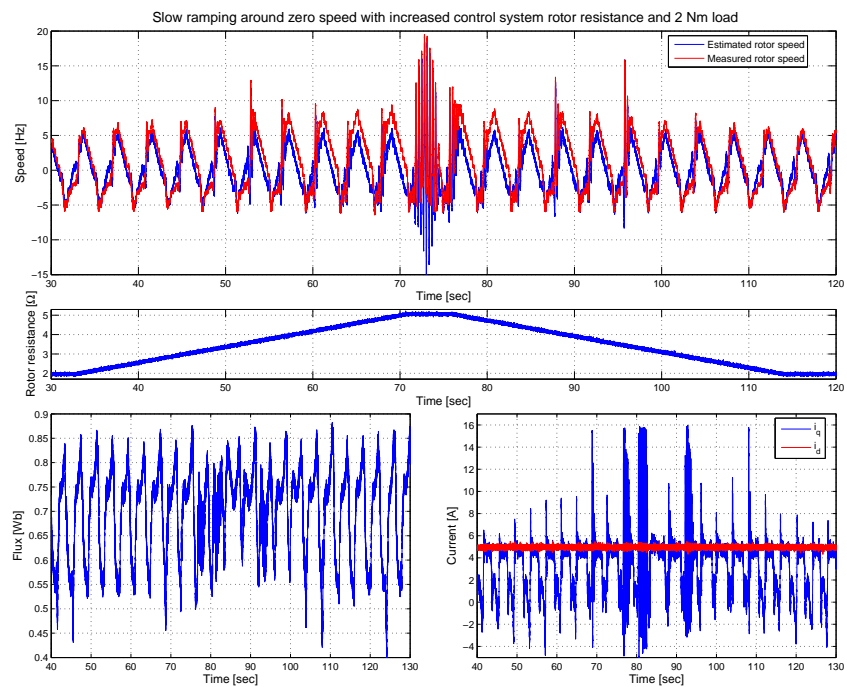


Figure 7.18: Speed, estimated flux and measured currents at ramped speed around zero as the control system rotor resistance is first increased, then lowered to the nominal value. The test is conducted twice, first to log speeds and resistance and secondly to log flux and currents.

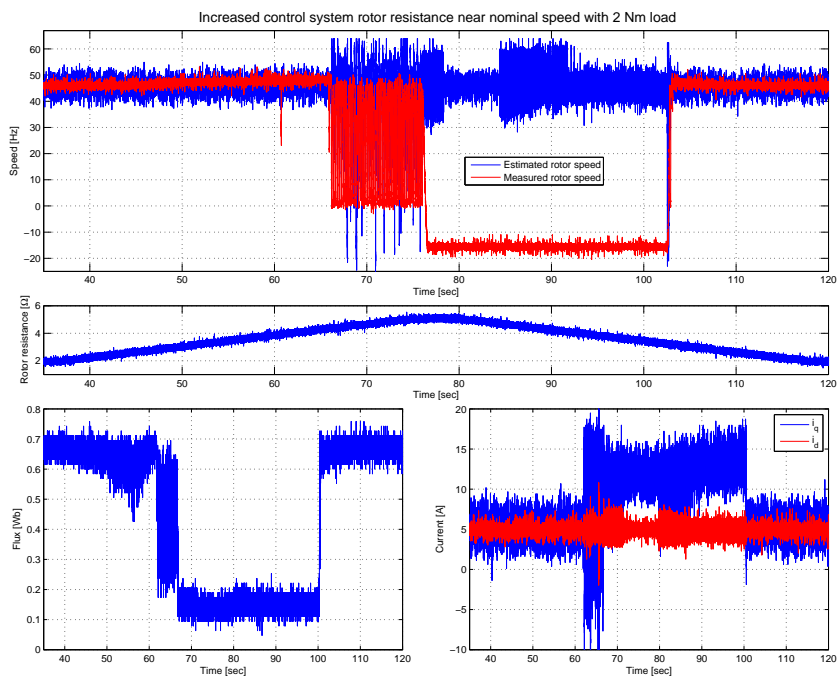


Figure 7.19: Speed, estimated flux and measured currents at near nominal speed as the control system rotor resistance is first increased, then lowered to the nominal value. The test is conducted twice, first to log speeds and resistance and secondly to log flux and currents.

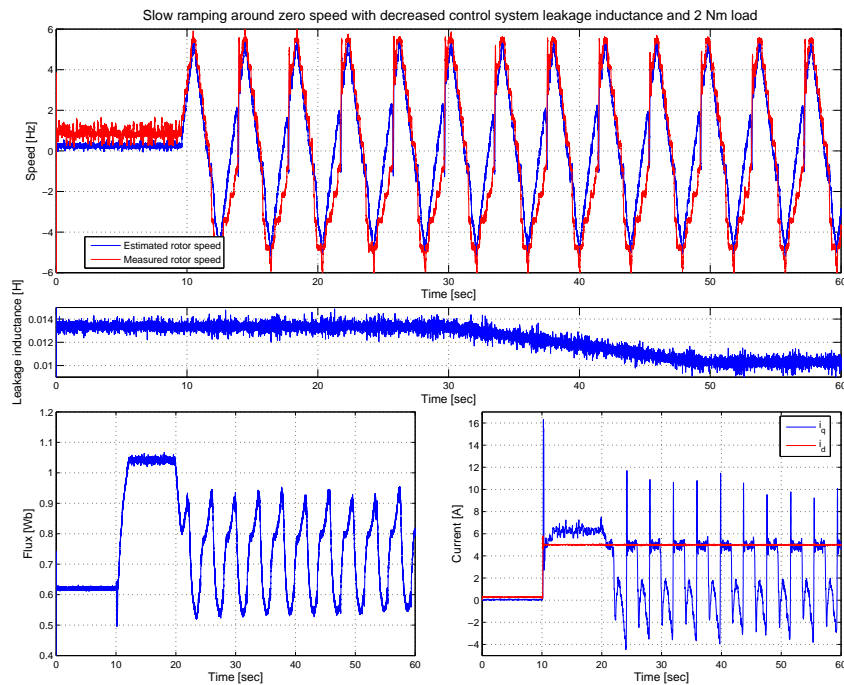


Figure 7.20: Speed, estimated rotor flux and measured currents at speed ramped about zero as the control system leakage inductance is decreased. A lower inductance means emulating an increase of motor inductance. The test is conducted twice, first to log speeds and inductance and secondly to log flux and currents.

### 7.3.3 Deviations in Leakage Inductance

As may be seen from Figures 7.20-7.23, the drive is quite unaffected as the total leakage inductance is changed.

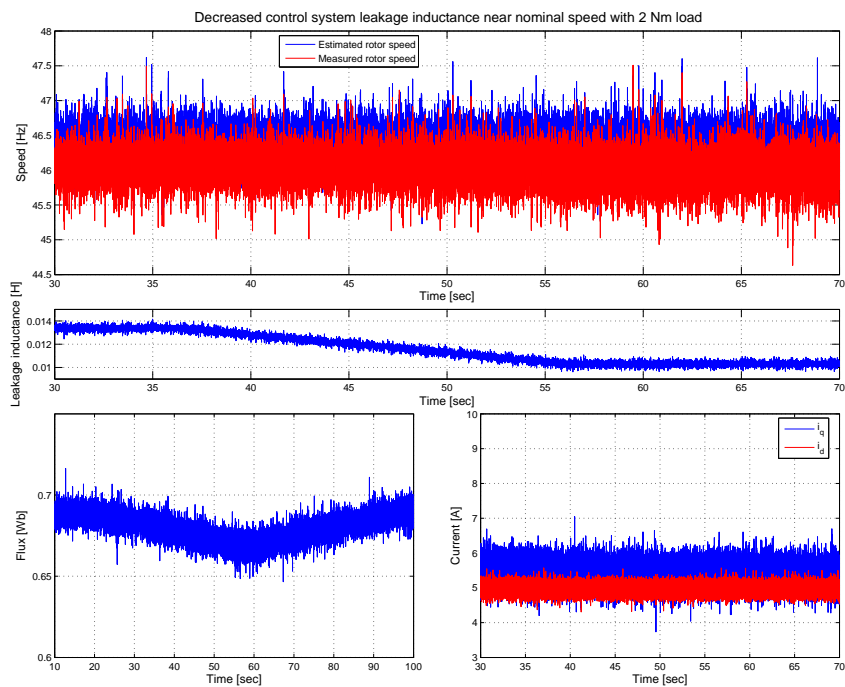


Figure 7.21: Speed, estimated rotor flux and measured currents at near nominal speed as the control system leakage inductance is decreased. A lower inductance means emulating an increase of motor inductance. The test is conducted twice, first to log speeds and inductance and secondly to log flux and currents.

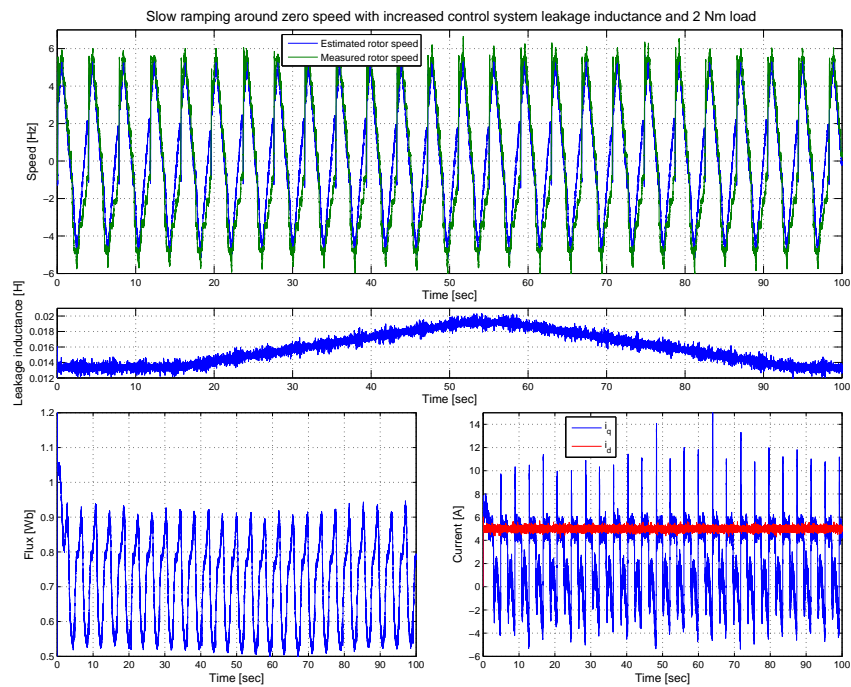


Figure 7.22: Speed, estimated flux and measured currents at ramped speed around zero as the control system leakage inductance is increased. The test is conducted twice, first to log speeds and inductance and secondly to log flux and currents.

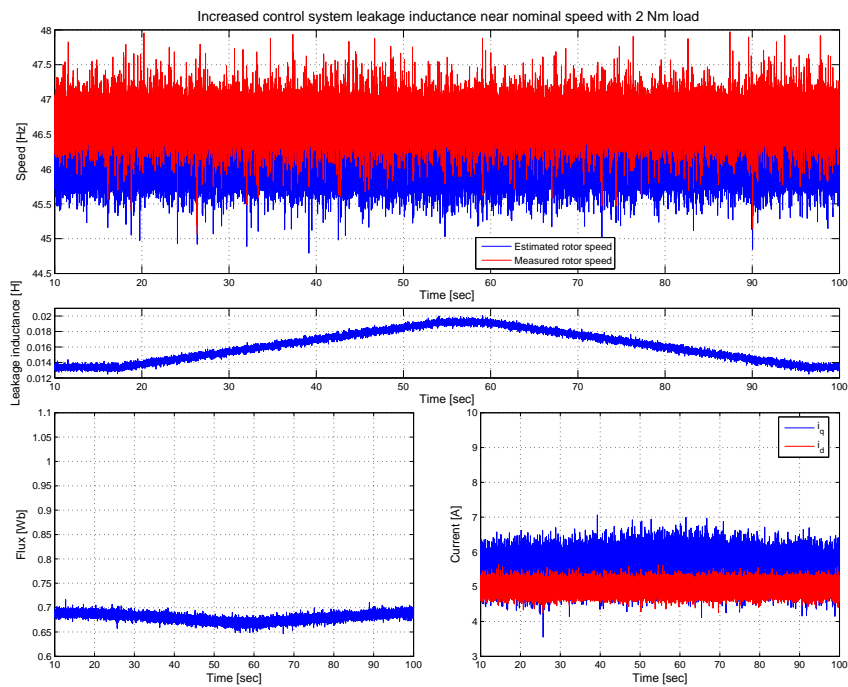


Figure 7.23: Speed, estimated flux and measured currents at near nominal speed as the control system leakage inductance is increased. The test is conducted twice, first to log speeds and inductance and secondly to log flux and currents.

# Chapter 8

## Conclusions

The implementation of the Statically Compensated Voltage Model was completed with some success. As shown in Chapter 7, the goals were partly met.

### 8.1 Goal Fulfilment

In this section, the results are compared to the set goals.

#### 8.1.1 Stable Operation up to Nominal Speed

The drive works well at nominal speed. Low speed operation is more problematic. Keeping zero speed is not possible with the implemented design. At slow operation, the accuracy is reduced. Slow braking is possible with 2 Nm load but not with nominal load, 3.7 Nm, where it is unstable already at 7.5 Hz.

#### 8.1.2 Stable Operation up to Twice the Nominal Torque

It has been shown that the SCVM is capable of handling large loads at nominal speeds. The limitations are more dependent on the inverter design and the power source present. At low speed, larger loads are not possible.

#### 8.1.3 Stable Operation during Acceleration and Deceleration with an Arbitrary Load

Slow reversal with more than moderate load is not possible. The problems occur in the braking mode.

#### 8.1.4 Stable Operation during Parameter Variations

As the motor parameters are not controllable, changes in motor data are emulated by changing the control system parameters. In this way, the control

system is put through similar stress as if the real motor parameters change.

- The drive is sensitive to changes in the value of the stator resistance. It is stable for variations between -37 % and +60 % in low speed operation. In the high speed region, the drive is less sensitive to stator resistance deviations. It can handle a discrepancy of  $\pm 60$  % before becoming unstable.
- The rotor resistance may decrease by 58 % at low speed and by 53 % at nominal speed before the drive destabilizes. Increasing the rotor resistance with 60 % will not affect the stability at any speed but the nominal speed accuracy will be reduced by approximately 2 %.
- The implemented design is capable of handling deviations with 30 % in the total leakage inductance without any noticeable effect on performance at any speed.

## 8.2 Further Work

To improve the drive, one important contribution would be an on-line parameter estimator. A good solution should be easy to understand and implement. On-line tuning would also minimize the risk of failing units due to scatter in motor parameters. It may also open the possibility for a stand-alone sensorless drive, ready for operation with almost any IM within its power range. The effects of parameter variations could perhaps be less by implementing the suggested improvements in Section 4.3.

## Appendix A

# Measurement of Motor Parameters

Two types of tests were conducted; a locked-rotor test to determine  $R_r$ ,  $L_r$  and  $L_s$  and a no load test to get  $L_m$ . The stator resistance  $R_s$  was measured directly on the motor terminals. All measurements are performed on a relatively cold motor.

The motor is produced by Bonfiglioli Group and is marked with the data found in table A.1. From these data, the approximate nominal flux level is calculated by

$$T = i_q \lambda_r \quad (\text{A.1})$$

$$T = \frac{P}{\omega_r} \quad (\text{A.2})$$

$$\lambda_r = \frac{P}{\omega_r i_q}. \quad (\text{A.3})$$

With the parameters from table A.1, the approximate nominal flux level for this motor is  $\lambda_{dr}^* = 0.605\text{Wb}$ .

The motor-bench at Aros electronics AB is equipped with a Panasonic MSMA402A1G AC servo motor (serial no: 03090001F) which is used as load. An Infratek 106A Power Analyzer (serial no: 03083312) is used for measuring currents, voltage, active power, apparent power and power factor.

V $\Delta$ / Y	Hz	kW	A $\Delta$ / Y	rpm	$\cos(\phi)$
230/400	50	1.1	4.41/2.55	2815	0.81
—/460	60	1.3	—/2.5	3420	

Table A.1: Motor data from nameplate.

$I_a$ (A)	$P_{tot}$ (W)	$S_{tot}$ (VA)	$Q_{tot}$ (VAR)	$\frac{L_{lr}+L_{ls}}{2}$ (mH)	$R_r$ ( $\Omega$ )
1.02	12.63	18.29	13.23	6.75	2
2.01	49.05	71.53	52.06	6.84	2
3.01	110.19	160.07	116.11	6.80	2.01
4.06	203.52	292.97	210.74	6.78	2.07
5.04	310.48	447.57	322.37	6.78	2.02

Table A.2: Results from locked rotor test.

## A.1 Locked Rotor Test

With the rotor locked, the slip is equal to one. This gives minimum effective rotor resistance, thus minimizing the current through the magnetizing inductance, which may be neglected. The motor steady-state T model equivalent circuit is then reduced to figure A.1. The rotor of the IM was locked by applying a large braking torque on the servo. The current was increased in steps and the required voltage noted together with apparent power and active power. The reactive power is calculated from

$$Q_{tot} = \sqrt{S_{tot}^2 - P_{tot}^2}. \quad (\text{A.4})$$

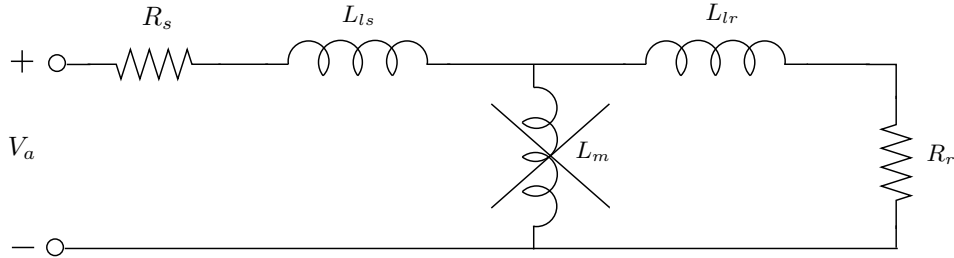


Figure A.1: Reduced T-model for locked rotor test.

The rotor and stator inductances  $L_{lr}$  and  $L_{ls}$  are assumed equal. The reactive power is then equal to

$$Q_{phase} = \omega(L_{lr} + L_{ls})I_a^2 \quad (\text{A.5})$$

where  $Q_{phase} = Q_{tot}/3$ . The result of the measurements is found in table A.2.

The mean value of these tests yields  $L_{ls} = L_{lr} = 6.79$  (mH). Using the measured stator resistance,  $R_s = 2.05$  ( $\Omega$ ), the rotor resistance,  $R_r$ , can be calculated using the measured active power

$$P_{phase} = (R_r + R_s)I_a^2. \quad (\text{A.6})$$

The mean value of  $R_r = 2.02$  ( $\Omega$ ).

$I_a$ (A)	$P_{tot}$ (W)	$S_{tot}$ (VA)	$Q_{tot}$ (VAr)	$L_m$ (mH)
2.83	143.36	1134.3	1125.2	144.6
2.95	153.79	1192.5	1182.5	139.7
2.91	148.20	1170.3	1160.9	140.6

Table A.3: Results from no-load test.

## A.2 No-load Test

Nominal voltage is supplied to the motor. The servo motor drives the IM at synchronous speed to control the slip speed to zero. The effective rotor resistance becomes large and can be neglected. The equivalent circuit is seen in figure A.2. Current, active power, apparent power and power factor

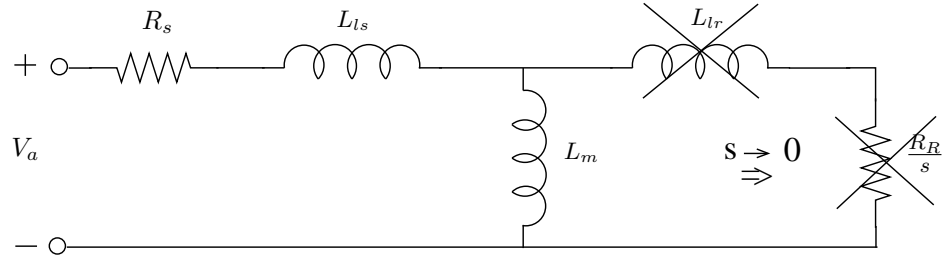


Figure A.2: Reduced T-model for locked rotor test.

is noted.

The current  $I_a$  splits between the magnetizing inductance  $L_m$  and the core loss resistance  $R_c$  according to

$$I_m = \sin(\phi)I_a. \quad (\text{A.7})$$

To extract the magnetizing inductance  $L_m$ , the following relation is used:

$$Q_{phase} = I_a^2 \omega_1 L_{l_s} + I_m^2 \omega_1 L_m \quad (\text{A.8})$$

The values from the power analyzer is read three times with aid of a hold function. The test results can be found in table A.3. The mean value of the magnetizing inductance is found to be 141.6 mH.

# Bibliography

- [1] A. Ottergren, “Evaluation of speed observers for an induction machine,” Master’s thesis, Department of Electric Power Engineering, Chalmers University of Technology, Gothenburg, 2003.
- [2] L. Harnefors, *Control of Variable-Speed Drives*. Västerås, Sweden: Department of Electronics, Mälardalen University, 2002.
- [3] ———, *Control of Power Electronic Converters and Variable-Speed Drives*. Västerås, Sweden: Department of Electronics, Mälardalen University, 2005.
- [4] G. R. Slemon, “Modelling of induction machines for electric drives,” *IEEE Transactions on Industry Applications*, vol. 25, no. 6, pp. 1126–1131, November/December 1989.
- [5] R. Krishnan, *Electric Motor Drives*. Upper Saddle River, New Jersey: Prentice Hall, 2001.
- [6] M.-H. Shin, D.-S. Hyun, S.-B. Cho, and S.-Y. Choe, “An improved stator flux estimation for speed sensorless stator flux orientation control of induction motors,” *IEEE Transactions on Power Electronics*, vol. 15, no. 2, pp. 312–318, March 2000.
- [7] R. Ottersten, “On control of back-to-back converters and sensorless induction machine drives,” Ph.D. dissertation, Department of Electric Power Engineering, Chalmers University of Technology, Gothenburg, 2002.
- [8] N. Mohan, *Electric Drives*. Minneapolis, Minnesota: MNPERE, 2003.

